5 Modelling nitrogen dynamics around a burrow

5.1 Introduction

Burrow irrigation by thalassinidean shrimp serves several functions, including sediment and waste expulsion and, in some cases feeding (eg. Stapleton et al. (2002)). A key role is to draw oxygenated water into the burrow system. While many of these animals can tolerate low oxygen levels, and even prolonged periods of anoxia (Paterson and Thorne (1995)), they do need to respire aerobically within their burrows. The introduction of oxygen into sediment depths profoundly influences the surrounding sediment chemistry, with the effects plainly visible in many cases (eg. Figure 1.5).

The modelling work in this chapter aimed at investigating the effect of burrow irrigation on nitrogen dynamics, and to make some more specific predictions about the impact of thalassinidean shrimp behaviour. A further aim was to model the sediments of Port Phillip Bay to investigate the role that irrigated burrows could play in observed denitrification rates. Section 5.3 describes the model development, Section 5.4 outlines some general model behaviour, Section 5.5 investigates three thalassinidean shrimp case studies, and Section 5.6 describes the Port Phillip Bay modelling.

5.2 Background

Burrows serve to increase the area of the oxic-anoxic interface, thus altering the redox zonation geometry (Figure 5.1) and potentially increasing the number of sites suitable for coupled nitrification-denitrification reactions.

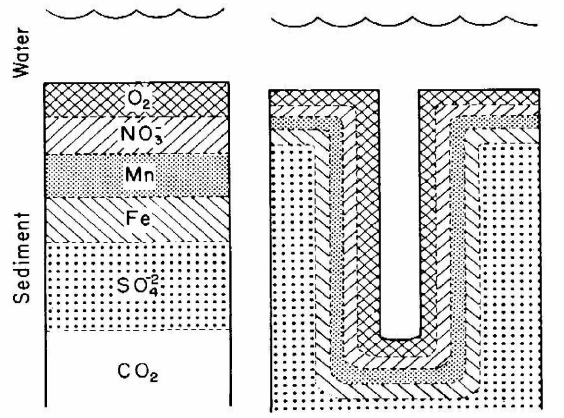

Figure 5.1 Diagram from Aller (1982) demonstrating the potential impact of burrow irrigation on redox zonation in sediments.

Aller (1980) used a cylindrical burrow model to illustrate the likely effect of irrigated burrows on distributions of porewater species. The cylinder model takes the following form (assuming zero advection velocity):

$$\frac{\partial C}{\partial t} = D_s \frac{\partial^2 C}{\partial z^2} + \frac{D_s}{r}\frac{\partial}{\partial r} r \frac{\partial C}{\partial r} + R(C, z, r) \qquad \textbf{(5.1)}$$

where z is vertical distance from the sediment surface, r is the horizontal distance from the burrow centre, C is the concentration, D_s is the molecular diffusion coefficient corrected for tortuosity and R is a reaction term. Typical boundary conditions are

$$\begin{aligned} C &= C_0 \quad z = 0 \\ C &= C_0 \quad r = r_1 \\ \frac{\partial C}{\partial r} &= 0 \quad r = r_2 \\ \frac{\partial C}{\partial z} &= B \quad z = L \end{aligned} \qquad \textbf{(5.2)}$$

where r_1 is the radius of the burrow, r_2 is the outer radius of the sediment annulus surrounding the burrow and L is the depth of the burrow. B is a prescribed flux.

Aller (1988) used a modified version of this approach to model the nitrogen dynamics surrounding an irrigated burrow. The main modification was to represent two zones in the sediment: an oxic annulus of sediment surrounding the burrow (Zone 1), surrounded by an anoxic annulus of sediment (Zone 2). Analytical solutions were investigated for two species: NH_4^+ and NO_3^-. The NH_4^+ case assumed that NH_4^+ was produced only in Zone 2 according to zeroth order kinetics (and no nitrification in the oxic zone). The NO_3^- case assumed zeroth order nitrification in Zone 1 and first order denitrification in Zone 2, as well as zeroth order nitrification exponentially decreasing with depth, to avoid having to represent two layers in the vertical direction as well as radial direction.

Some of the main findings from the work are briefly mentioned here. Firstly, irrigated burrows profoundly influenced the distribution of species with zeroth order production terms, such as NH_4^+. Burrow separation distance was a particularly important control on NH_4^+ concentration in the model. Unless nitrification regions directly overlapped, denitrification was increased when burrows were present. The ratio of denitrification to nitrification was also altered by the presence of burrows, usually increasing.

The approach used in this chapter was influenced by Aller's work. I coupled a simple nitrogen dynamics model (based on Blackburn and Blackburn (1993)) to a radially-symmetrical burrow irrigation model. Advantages of this approach include the fact that the oxic and anoxic zones are no longer user-prescribed but determined by the model itself (oxygen is one of the species modelled), and nitrification and denitrification are represented by more realistic reaction terms. The aim of this work was to apply a burrow irrigation model to some specific case studies. The main findings from Aller's founding work remain unchanged, and in general his analytical solutions are the most elegant approach for investigating fundamental issues of interactions between model geometry and reaction kinetics.

5.3 Model description

The aim of this work was to develop irrigation models that allow for time-varying, incomplete burrow flushing and coupled chemical reactions. Most of the cases considered in this chapter are modelled using a one-dimensional radial model. The model simulates a one-dimensional transect radiating out from the burrow centre, assuming radial symmetry. The simplification is justified because the burrow lengths of interest are long and along-burrow variation is expected to be minor relative to variations in the radial direction. This implicitly assumes that the sediment surface is sufficiently far away so that it does not influence the reactions. This assumption is investigated in Section 5.6.2.

Modelling more complicated irrigation behaviour presents many challenges, particularly as measurements of burrow chemistry and irrigation behaviour are scarce. The temptation is to include a number of processes that common sense suggest must be occurring within the burrow, however in the absence of constraining data these inclusions merely add convenient parameters which can be tweaked endlessly to achieve novel results. Every attempt has been made to minimise this possibility. Where possible, parameters are constrained by published measurements and are not allowed to deviate from these. The remaining unconstrained parameters are discussed in each case.

The model was constructed in Matlab, using the method of lines. The one-dimensional diffusion equation in cylindrical polar coordinates was represented by a central difference finite difference approximation in space, hence reducing the system of coupled partial differential equations to a set of coupled ordinary differential equations

(ODEs). Matlab's stiff ODE solver, 'ode15s', was used to solve the system of equations. The solver's performance was improved by specifying a sparse analytical Jacobian matrix for the system of equations, and modifying 'ode15s' to perform a column permutation prior to any LU decompositions (matrix decomposition to a product of upper and lower triangular matrices). The Jacobian matrix of a system of ordinary differential equations, $\frac{\mathrm{d}\mathbf{y}}{\mathrm{d}t} = \mathbf{f}(\mathbf{y})$ is defined as:

$$J = \begin{bmatrix} \frac{\partial f_1}{\partial y_1} & \frac{\partial f_1}{\partial y2} & \cdots \\ \frac{\partial f_2}{\partial y_1} & \frac{\partial f_2}{\partial y_2} & \cdots \\ \vdots & \vdots & \ddots \\ & & \end{bmatrix}$$

where $\mathbf{y} = [y_1, y_2, y_3, \ldots]$ and $\mathbf{f}(\mathbf{y}) = [f_1(\mathbf{y}), f_2(\mathbf{y}), f_3(\mathbf{y}), \ldots]$.

A dissolved species at grid location i is modelled by the following equation:

$$\frac{\partial C_i}{\partial t} = D\frac{\partial^2 C_i}{\partial r^2} + \frac{D}{r_i}\frac{\partial C_i}{\partial r} + R \qquad \textbf{(5.3)}$$

and is represented by the following finite difference approximation in the model:

$$\frac{\mathrm{d}C_i}{\mathrm{d}t} = D\frac{C_{i+1} - 2C_i + C_{i-1}}{\Delta r^2} + \frac{D}{r_i}\frac{C_{i+1} - C_{i-1}}{2\Delta r} + R(C_i) \qquad \textbf{(5.4)}$$

where C_i is the porewater concentration at grid location i, Δr is the grid step, D is the rate of diffusion and R is the reaction term. This formulation assumes constant porosity in the sediment. The model allows for a finer grid to be prescribed on both sides of the burrow wall, so allowing greater spatial resolution at this interface. At the interface between two grid sizes, second order finite difference formulas for an uneven grid were used (Boudreau (1997) p. 326):

$$\left.\frac{\partial \mathrm{C}}{\partial r}\right|_{r_i} = -\frac{\Delta r_{i+1}}{\Delta r_i(\Delta r_i + \Delta r_{i+1})}C_{i-1} + \frac{\Delta r_{i+1} - \Delta r_i}{\Delta r_i \Delta r_{i+1}}C_i + \frac{\Delta r_i}{\Delta r_{i+1}(\Delta r_i + \Delta r_{i+1})}C_{i+1} \qquad \textbf{(5.5)}$$

and

$$\left.\frac{\partial^2 C}{\partial r^2}\right|_{r_i} = \frac{2}{\Delta r_i(\Delta r_i + \Delta r_{i+1})} C_{i-1} - \frac{2}{\Delta r_i \Delta r_{i+1}} C_i + \frac{2}{\Delta r_{i+1}(\Delta r_i + \Delta r_{i+1})} C_{i+1} \quad \textbf{(5.6)}$$

where $\Delta r_{i+1} = r_{i+1} - r_i$.

Seven chemical species, oxygen (O_2), nitrate (NO_3^-), sulfate (SO_4^{2-}), dissolved organic carbon (DOC), ammonium (NH_4^+), nitrogen gas (N_2) and sulfide (HS^-) were modelled using the kinetics based on those described in Blackburn and Blackburn (1993). The model assumes that reactions only occur within the sediment, so $R = 0$ for all species in the burrow water. Twelve species were represented in their model: carbon dioxide (CO_2), dissolved organic carbon (DOC), dissolved organic nitrogen (DON), HS^-, NH_4^+, exchangeable ammonium (NH_4_ex), NO_3^-, N_2, particulate organic carbon (POC), particulate organic nitrogen (PON), O_2 and SO_4^{2-}. The reasons for omitting five of the species are varied. The distributions of nitrogen species take the same shape as the distributions of carbon species, varying only by a known factor (the carbon to nitrogen ratio), so PON and DON can be omitted. POC was omitted and its function was replaced with a production rate of DOC (P_{DOC}) which specifies the rate and distribution of DOC production. CO_2 was omitted, as its exclusion does not affect the distributions of other species. A model version was constructed which included exchangeable ammonium, however there was negligible difference in results when it was excluded from the model. The original authors of the model have also routinely omitted NH_4_ex from their model formulation (eg. Blackburn and Henriksen (1983), Blackburn et al. (1994)).

The equations for the remaining species reaction rates are:

$$\begin{aligned}
R_{O_2} &= -k_3 O_{2_stim}[DOC] - 2k_6 O_{2_stim}\left[NH_4^+\right] - 2k_7 O_{2_stim}\left[HS^-\right] \\
R_{NO_3^-} &= -k_4 NO_{3_stim} O_{2_inhib}[DOC] + k_6 O_{2_stim}\left[NH_4^+\right] \\
R_{SO_4^{2-}} &= -k_5 SO_{4_stim} O_{2_inhib}[DOC] + k_7 O_{2_stim}\left[HS^-\right] \\
R_{DOC} &= P_{DOC} - k_3 O_{2_stim}[DOC] - 2k_5 SO_{4_stim} O_{2_inhib}[DOC] \\
&\quad -1.25 k_4 NO_{3_stim} O_{2_inhib}[DOC] \\
R_{N_2} &= 0.5 k_4 NO_{3_stim} O_{2_inhib}[DOC] \\
R_{NH_4^+} &= k_3 O_{2_stim} \frac{[DOC]}{\lambda_{CN}} + 1.25 k_4 NO_{3_stim} O_{2_inhib} \frac{[DOC]}{\lambda_{CN}} \\
&\quad +2k_5 SO_{4_stim} O_{2_inhib} \frac{[DOC]}{\lambda_{CN}} - k_6 O_{2_stim}\left[NH_4^+\right] \\
R_{HS^-} &= k_5 SO_{4_stim} O_{2_inhib}[DOC] - k_7 O_{2_stim}\left[HS^-\right]
\end{aligned} \quad \textbf{(5.7)}$$

where square brackets represent porewater concentration. λ_{CN} is the carbon to nitrogen ratio (assumed to follow Redfield C:N stoichiometry of 106:16). The rate constants are the same as those specified by Blackburn and Blackburn (1993): k_3 = 30 d^{-1} for DOC oxidation by O_2; k_4 = 30 d^{-1} for DOC oxidation by NO_3^-; k_5 = 5 d^{-1} for DOC oxidation by SO_4^{2-}; k_6 = 30 d^{-1} for NH_4^+ oxidation by O_2 (nitrification); k_7 = 200 d^{-1} for HS^- oxidation by O_2. The _stim and _inhib functions are:

$$C_{\_stim} = \begin{cases} \dfrac{[C]}{C_{crit}} & [C] < C_{crit} \\ 1 & \text{otherwise} \end{cases} \qquad \textbf{(5.8)}$$

$$O_{2\_inhib} = \begin{cases} 1 - \dfrac{[O_2]}{C_{crit}} & [O_2] < C_{crit} \\ 0 & \text{otherwise} \end{cases}$$

where C_{crit} is 30 nmol/cm^3.

Molecular diffusion coefficients were corrected for temperature and salinity, where known. In the absence of this information, the diffusion coefficients given in Blackburn and Blackburn (1993) were used. These molecular diffusion coefficients were further corrected for tortuosity within the sediment. The choice of diffusion coefficient in the burrow itself varied. In some cases simply the molecular diffusion coefficients in water were used, but in other cases it made more sense to assume a higher rate of mixing within the burrow (due to animal movement). In these cases diffusion rates were set to be a factor of 10 higher than molecular diffusion rates. These details were found to make little difference to model results.

A no-flux boundary condition applies at the far boundary ($r = r_2$), which is equivalent to assuming that there is no flux between burrows:

$$\left.\frac{\partial C}{\partial r}\right|_{r=r_2} = 0 \qquad \textbf{(5.9)}$$

Radial symmetry allows us to assume that concentration distributions have a local maximum or minimum at the burrow centre, so

$$\left.\frac{\partial C}{\partial r}\right|_{r=0} = 0 \qquad \textbf{(5.10)}$$

Three forms of irrigation behaviour were modelled:

1) Constant, fully flushed burrow (burrow water concentrations identical to surface water concentrations). In this case, the burrow region is not included in the model (as it is simply a uniform concentration) and a constant-concentration boundary condition applies at $r = r_1$.

2) Oscillating irrigation conditions. Irrigation behaviour is specified using a period (T_i) and an irrigation fraction (p_i). The irrigation fraction p_i is the fraction of time that is spent flushing the burrow. For example, a burrow irrigated for 15 minutes every hour has $T_i = 1/24$ days and $p_i = 0.25$. During periods of burrow irrigation, the burrow water concentrations were held constant. The concentrations were calculated by assuming that the burrow water is mixed with an injection of surface water. For example, if C_q is the burrow concentration at the end of a quiescent period, the concentration assumed during the subsequent irrigation period is

$$C = fC_o + (1-f)C_q \qquad \textbf{(5.11)}$$

where C_o is the concentration in the overlying water and f is a mixing efficiency; it is the fraction of burrow volume that is replaced with overlying water during a flushing event.

3) Constant, partially flushed burrow. The equation within the burrow zone includes a sink term:

$$\frac{\partial C_i}{\partial t} = D\frac{\partial^2 C_i}{\partial r^2} + \frac{D}{r_i}\frac{\partial C_i}{\partial r} + F_l\left(C_0 - C_i\right) \qquad \textbf{(5.12)}$$

where F_l is a flushing time constant and C_0 is the overlying water concentration. The sink term represents the injection of overlying water and the expulsion of burrow water at a rate specified by F_l. The residence time of water in the burrow is $1/F_l$. By specifying irrigation in this way, we avoid the complication of oscillating conditions, yet still capture the fact that burrow concentrations differ from overlying water conditions.

Fluxes across the burrow surface, J_{bur}, can be calculated from the model, using the following equation:

$$J_{bur} = 2\pi r_1 \phi D_s \left.\frac{\partial C}{\partial r}\right|_{r=r_1} \quad \textbf{(5.13)}$$

Note that the above expression produces a rate per unit burrow length (eg. nmol/cm/day). It is easily converted to a flux per unit of planar sediment surface (referred to as J_r) by multiplying the burrow flux by burrow length (L) and number of burrows per unit area (N):

$$J_r = LNJ_{\text{bur}} \quad \textbf{(5.14)}$$

When the system is at steady state, J_{bur} can be calculated from the following integration:

$$J_{bur} = 2\pi\phi \int_{r1}^{r2} R r \, \mathrm{d}r \quad \textbf{(5.15)}$$

Equation (5.15) was used in preference to equation (5.13) as it is more accurate to numerically integrate across a large number of cells than to numerically differentiate using relatively few cells at the burrow wall.

Key model outputs of interest are the rates of nitrification and denitrification. Again, due to the model geometry, these are rates per unit burrow length (nmol/cm/day). The carbon mineralisation rate is:

$$R_{\text{C}} = 2\pi\phi \int_{r1}^{r2} P_{\text{DOC}} r \, \mathrm{d}r \quad \textbf{(5.16)}$$

The nitrification rate is

$$R_{Nit} = 2\pi\phi \int_{r_1}^{r_2} k_6 O_{2\_\text{stim}} [NH_4] r \, \mathrm{d}r \quad \textbf{(5.17)}$$

and the denitrification rate is

$$R_{Dnit} = 2\pi r_1 \phi D_s \left.\frac{\partial [2N_2]}{\partial r}\right|_{r=r_1} \quad \textbf{(5.18)}$$

or if the system is at steady state it is preferable to calculate the denitrifcation rate using the integral form,

$$R_{Dnit} = 2\pi \int_{r1}^{r2} \phi\left(2R_{N_2}\right) r \, \mathrm{d}\, r. \qquad \textbf{(5.19)}$$

It is often convenient to express nitrification and denitrification rates as a percentage efficiency, which is the proportion of nitrogen mineralisation which is occurring through the nitrification and denitrification pathways. If overlying water concentrations of NH_4^+ and NO_3^- are zero (ie mineralisation of sediment organic matter is the only source of nitrogen), the nitrification efficiency is:

$$E_{Nit} = \frac{\lambda_{CN} R_{Nit}}{R_C} \qquad \textbf{(5.20)}$$

and the denitrification efficiency is:

$$E_{Dnit} = \frac{\lambda_{CN} R_{Dnit}}{R_C} \qquad \textbf{(5.21)}$$

5.4 General model behaviour

This section outlines some general model behaviour with reference to key parameters, P_{DOC}, r_1, r_2 and F_l. The model outputs of interest are the concentrations of O_2, NO_3^- and NH_4^+ and the rates of nitrification and denitrification. Typical profiles for each of these are presented in Figure 5.2. In this example, the burrow has a radius of 3mm and is fully flushed with overlying water. Oxygen is totally consumed within a 7 mm of the burrow wall, and this defines the zone of nitrification (which requires oxygen and NH_4^+). NH_4^+ is zero at the burrow wall, as it is fully flushed with overlying water (which is set to have an NH_4^+ concentration of zero). The steady state distribution of NH_4^+ represents a balance between production from organic matter decay, reaction with oxygen and diffusion across the burrow wall. NO_3^- produced within the nitrification zone diffuses out in two directions, where it is either lost from the system through diffusion across the burrow wall or by reaction with organic matter in anoxic zones (denitrification). The zone of denitrification exists just beyond the zone of nitrification, and its size depends on the rate of supply of NO_3^- and the volume of anoxic sediment. There is some overlap between the nitrification and denitrification zones, so that denitrification occurs in the presence of very low oxygen concentrations;

real sediments are heterogeneous, and there will be anaerobic microsites existing in low oxygen areas.

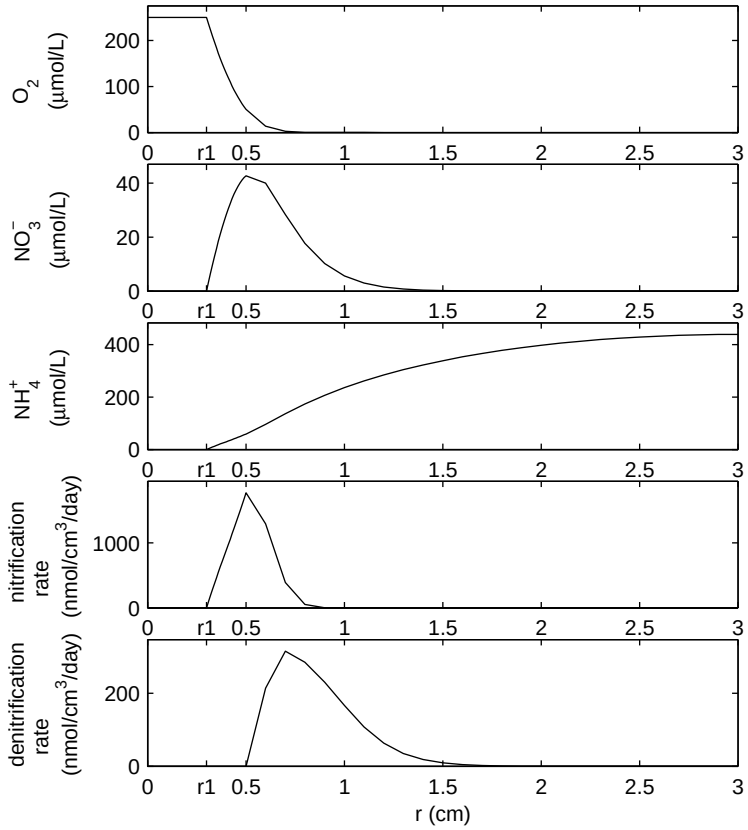

Figure 5.2 Typical profiles generated from the one-dimensional radial burrow model. The 3 mm radius burrow is fully flushed with overlying water ($[O_2]$ = 230 µmol/L, $[NO_3^-]=[NH_4^+]=0$). P_{DOC} was set at 500 µmol/L/day.

The effect of varying P_{DOC} for this model configuration is illustrated in Figure 5.3 and Figure 5.4. At very low values of P_{DOC} the oxygen penetrates to r_2, and so there are no anoxic regions in the sediment; no denitrification is possible under these circumstances. Nitrification rates are also low, as the rate of supply of NH_4^+ is low (the rate of supply of NH_4^+ is directly proportional to P_{DOC}). Nitrification efficiencies are 100% in these circumstances; no nitrogen leaves the system as DON or NH_4^+ because oxygen is readily available to react with both species. As P_{DOC} increases, an anoxic zone forms and denitrification becomes possible. For high oxygen penetration distances, the total denitrification rate is limited by the volume of anoxic sediment, and for low oxygen penetration distances the denitrification rate is limited by the amount of NO_3^- diffusing from the nitrification zone. The denitrification efficiencies peak at low P_{DOC} values, where nitrification rates are high but there is a small outer

anoxic zone where denitrification can occur. As P_{DOC} increases beyond this value, the nitrification and denitrification efficiencies decrease (Figure 5.4). This is because the rate of nitrification is overwhelmed by the rate of production of NH_4^+, and significant quantities of NH_4^+ leave the system through diffusion across the burrow wall.

The distance between burrows ($2r_2$) determines the amount of NH_4^+ that can build up in the sediment. This in turn affects the distributions of other species, and in particular it shifts the location of the oxic/anoxic boundary (Figure 5.5). Higher NH_4^+ concentrations fuel higher nitrification (and so denitrification) rates, however the efficiency of nitrification and denitrification decreases with increasing r_2 (Figure 5.6).

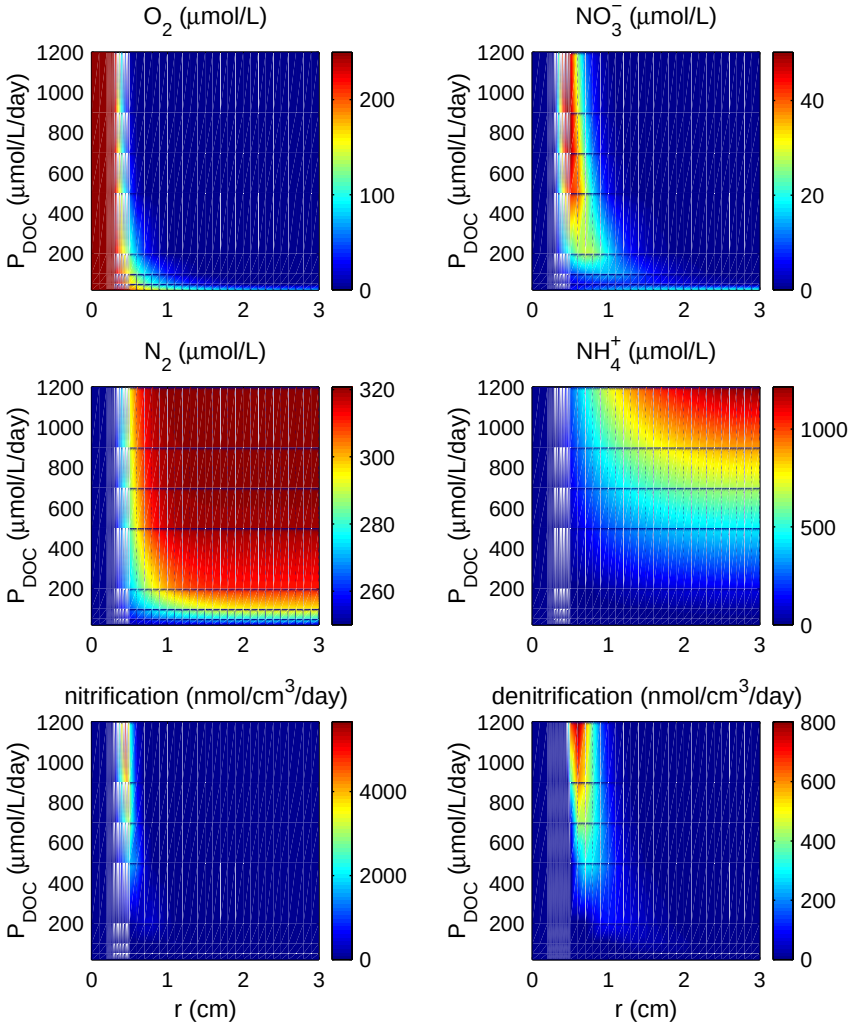

Figure 5.3 The effect of changing P_{DOC} on concentration and rate distributions.

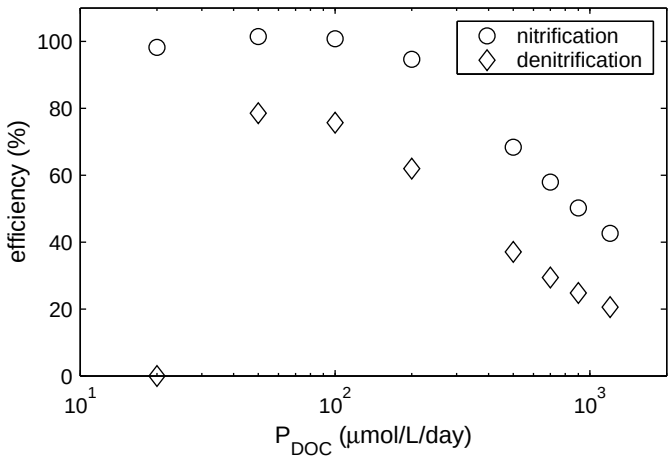

Figure 5.4 Changes in nitrification and denitrification efficiencies with changing P_{DOC} (all other parameters the same as example given in Figure 5.2).

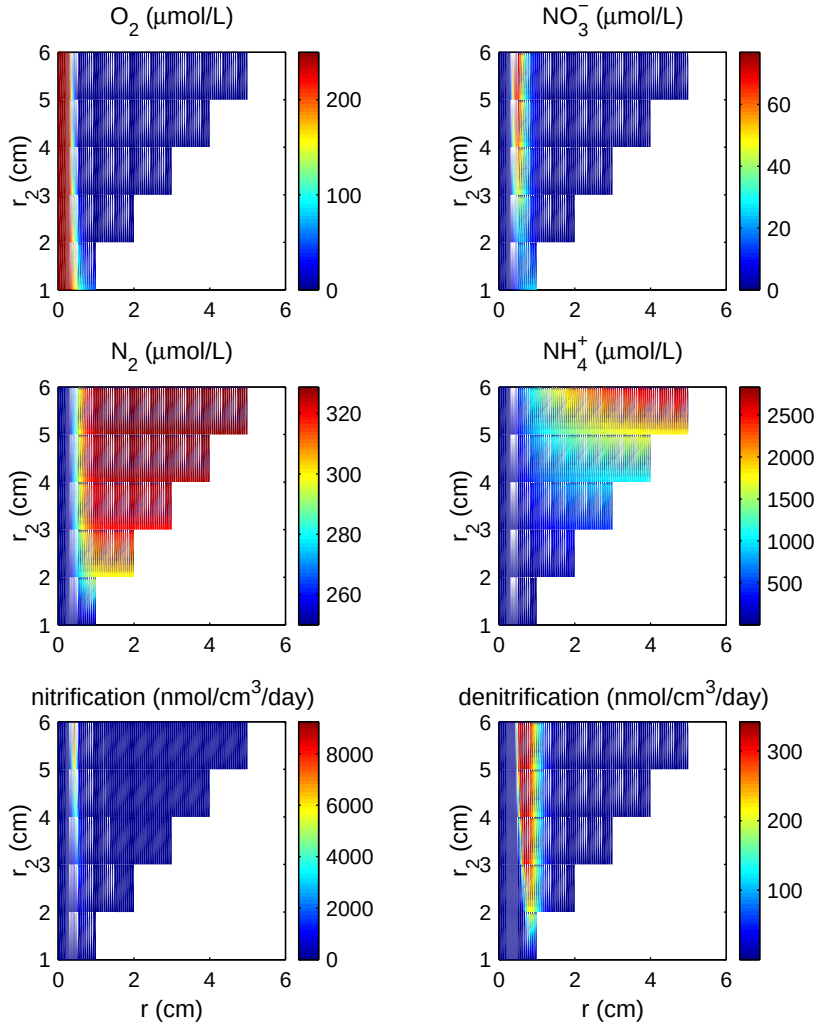

Figure 5.5 Effect of r_2 values on concentration and rate distributions.

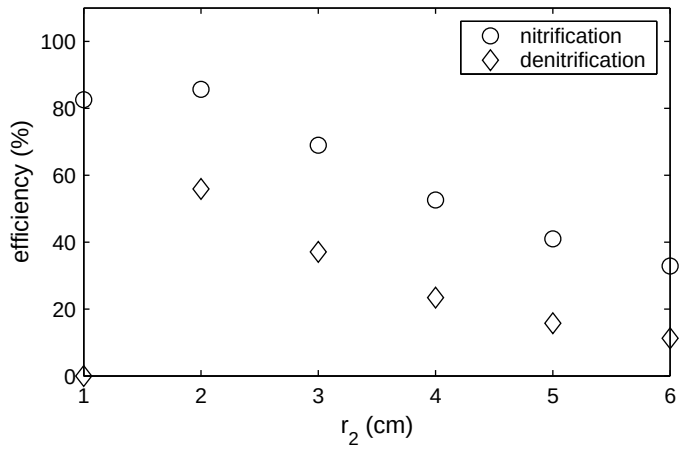

Figure 5.6 Changes in nitrification and denitrification efficiencies with changing r_2 (all other parameters the same as example given in Figure 5.2).

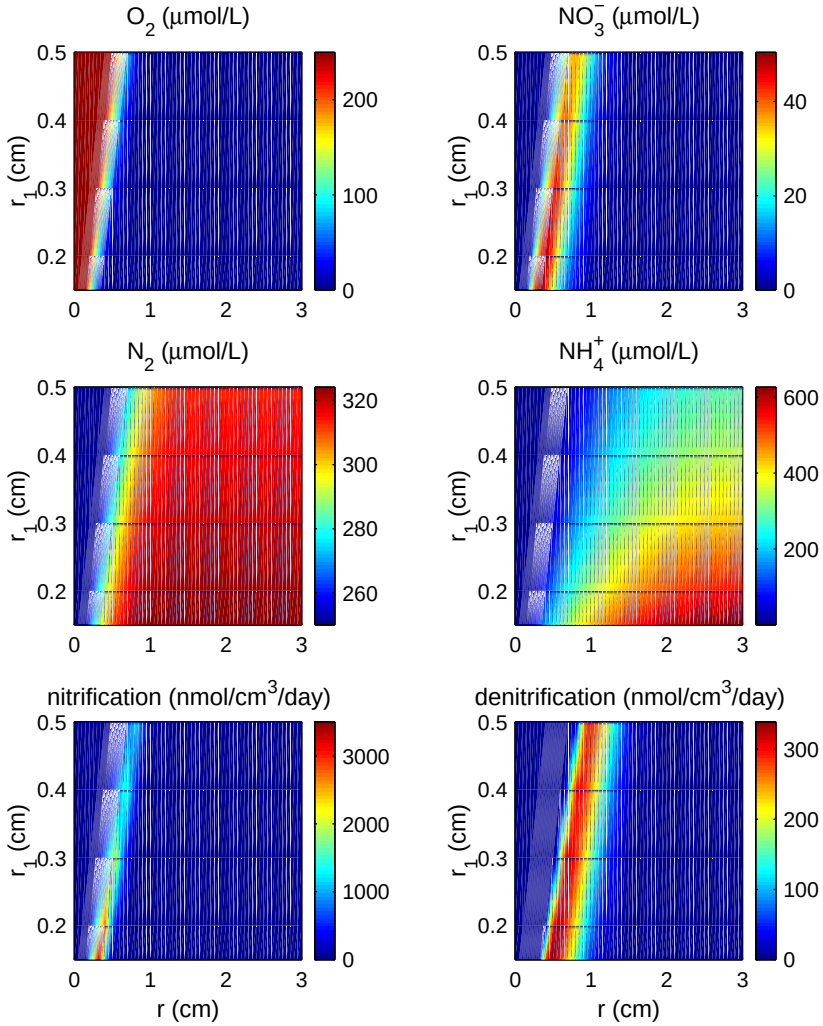

Figure 5.7 Effect of r_1 values on concentration and rate distributions for a fully flushed burrow.

The effect of changing the burrow radius, r_1 is not so pronounced for a fully-flushed burrow (Figure 5.7). Oxygen penetration increases with increasing r_1, creating a wider nitrification zone, and so slightly increasing nitrification (and denitrification) efficiencies (Figure 5.8). The effect is more pronounced for a partially flushed burrow. Under these circumstances, NH_4^+ and NO_3^- remain 'trapped' in the burrow after diffusing across the burrow wall. The amount trapped in the burrow strongly depends on the burrow volume (and so r_1), and this in turn affects the nitrification and denitrification efficiencies. For the same range of r_1 values, the partially flushed burrow produces a greater range of nitrification and denitrification efficiencies (although they are all lower than the fully flushed efficiencies).

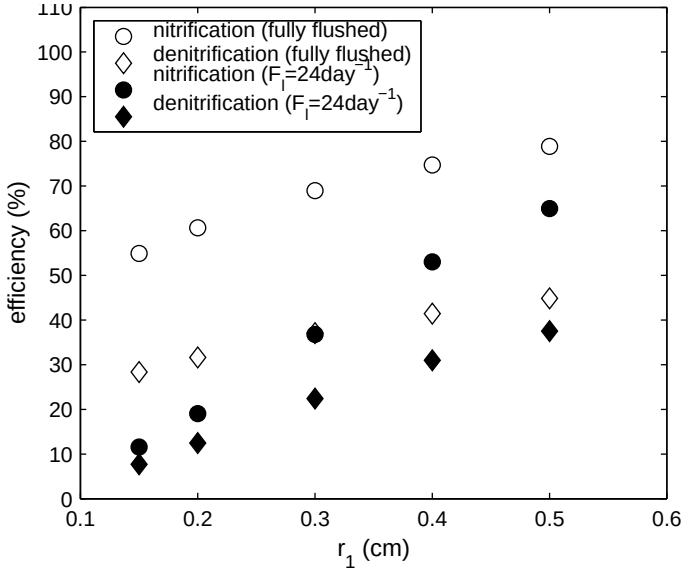

Figure 5.8 Changes in nitrification and denitrification efficiencies with changing r_1 for two burrow flushing rates (all other parameters the same as example given in Figure 5.2).

The effects of flushing rate are shown in Figure 5.9 and Figure 5.10. Nitrification efficiencies decrease with decreasing flushing rate as oxygen supply to the sediment is lowered. Denitrification efficiencies follow the same trend, as denitrification rates are limited by nitrification rates. A general summary of the model response to changing parameters is given in Table 5.1.

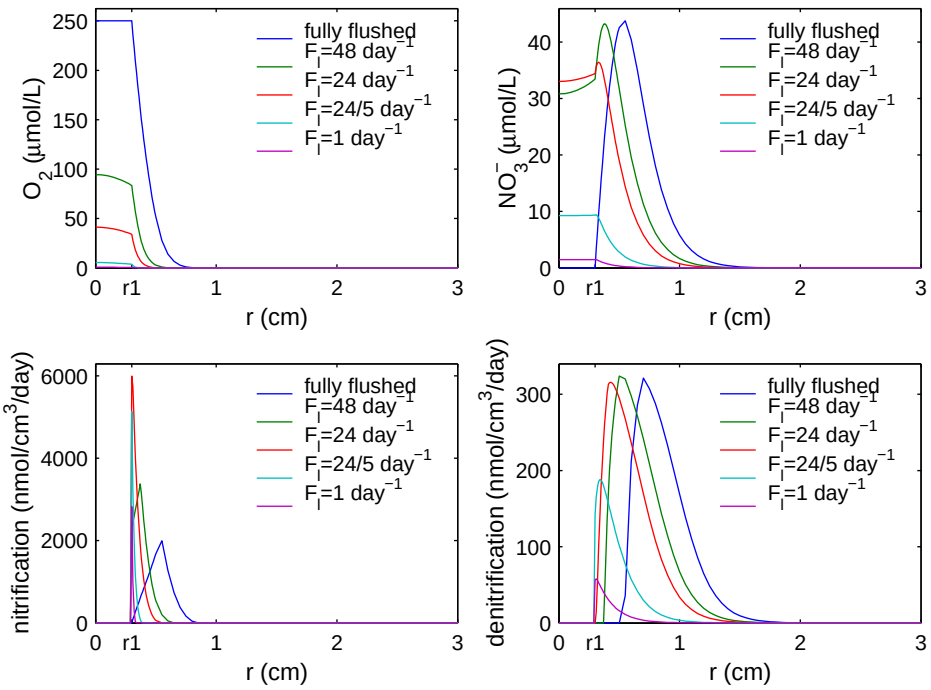

Figure 5.9 Effect of flushing rates on concentration and rate distributions.

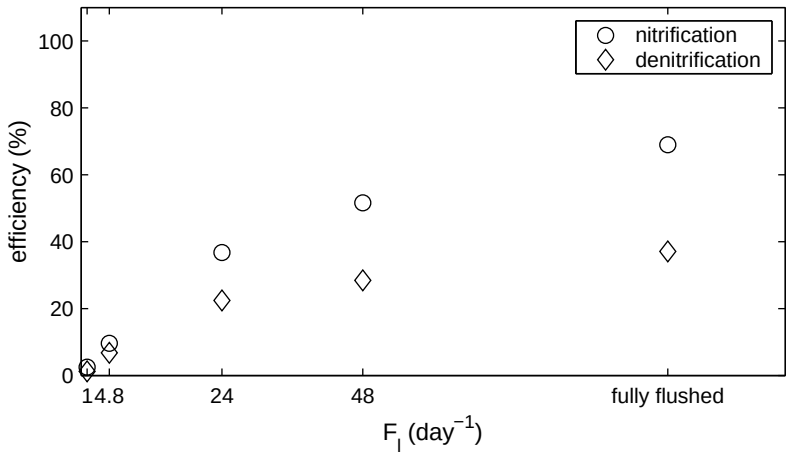

Figure 5.10 Changes in nitrification and denitrification efficiencies with changing flushing rates (all other parameters the same as example given in Figure 5.2.

Table 5.1 Directions of model response to parameter changes

	Maximum NH_4^+ concentration	**O_2 penetration distance**	**Nitrification efficiency**	**Denitrification efficiency**
Increasing P_{DOC}	Increases	Decreases	Decreases	Generally decreases
Increasing r_2	Increases	Decreases	Decreases	Decreases
Increasing r_1	Decreases	Increases	Increases	Increases
Increasing F_l	Decreases	Increases	Increases	Increases

In summary, nitrification efficiencies are high when the nitrification rate is high enough to keep up with NH_4^+ production. When the NH_4^+ production rate overwhelms the nitrification rate, ammonium builds up in the sediment surrounding the burrow, creating a steep gradient to the burrow wall and a high ammonium diffusive flux across the burrow wall. NH_4^+ production is controlled by P_{DOC}, and the distance r_2 is an important control on the amount of NH_4^+ that can accumulate in the system. Nitrification efficiency in turn is the main control on denitrification efficiency. Where nitrification efficiency is high, denitrification efficiencies will be high also, except for the situation when the nitrification zone approaches r_2, so there is little or no anoxic zone in which denitrification can occur.

5.5 Thalassinidean shrimp case studies

The aim of this section is to model some specific case studies drawn from the literature. There have been some excellent studies of thalassinidean shrimp burrow structure and burrow chemistry, and these provide an opportunity to test the modelling approach and compare theoretical understanding with actual measurements.

5.5.1 Case 1: modelling *Callianassa truncata* field data (Ziebis et al. (1996))

The measurements in *Callianassa truncata* burrows by Ziebis et al. (1996) are the only *in situ* measurements of thalassinidean shrimp burrow chemistry. A *Callianassa truncata* population was allowed to colonise the sediment surrounding a buried observatory in the Bay of Campese, Italy. My aim was to use their data to constrain model parameters in order to investigate the likely effect on nitrogen dynamics at depth.

The population was estimated at 120 burrow structures/m^2. Burrows consist of tubes (4-5 mm diameter) and chambers (14 mm diameter), and typically extend to depths of 50cm beneath the sediment surface. The authors estimated that the area of the sediment-water interface was increased by roughly 400%.

The sediment was sandy (porosity of 0.4) and poor in organic matter. The authors found that at a depth of 48 cm, burrow-water oxygen concentrations oscillated between 3% and 12% of air saturation. The period of oscillation was approximately one hour. The oxygen record at a depth of 26 cm showed no obvious periodicity, and oxygen levels were generally maintained between 10% and 40% of air saturation. Irrespective of sediment depth, oxygen penetration depths in the tube walls and spherical burrow chambers were approximately 3 mm and 7 mm respectively. Oxygen profiles measured in the laboratory suggested that oxygen penetration was 4mm at the sediment surface (away from burrow mounds). NH_4^+ levels were low in the burrow (2-14 μmol L^{-1}) and NH_4^+ was also depleted (<15 μmol L^{-1}) in the surrounding sediment to a radius of up to 3-4 cm.

Depth profiles of NH_4^+ levels were made in inhabited and uninhabited sediment. The uninhabited areas of sediment were established in mesh cages attached to the side of the observatory, and maximum values of approximately 100μmol/L were measured at depth (~50cm). Measurements were made two months after the observatory was deployed. Given that the sediment would have been mixed to remove animals and install the observatory, it seems reasonable to assume a uniform distribution of organic matter in the sediment column. I used a vertical (1-D planar) version of the nitrogen model to find a value of P_{DOC} that would produce NH_4^+ concentrations of ~100μmol/L after two months (P_{DOC} = 15 μmol/L/d). The surface oxygen penetration predicted by this scenario is large (~ 3cm), and far exceeds the 4mm penetration depth suggested by the authors. It should be noted that oxygen penetration at the surface was not measured *in situ*, and the penetration depth was inferred from measurements in a laboratory flume. Further, the NH_4^+ concentrations are zero to a depth of 10cm in the field measurements (Figure 5.11), which suggests even deeper oxygen penetration than that predicted by the model. In short, there is a contradiction between the laboratory measurements of oxygen (which suggest a 4 mm oxygen penetration depth) and the field measurements of NH_4^+ (which imply a 10 cm oxygen penetration depth) that cannot be explained by my model (which predicts a 3 cm oxygen penetration depth). A possible explanation for these differences is high levels of pore-water advection in the upper section of the field sediment.

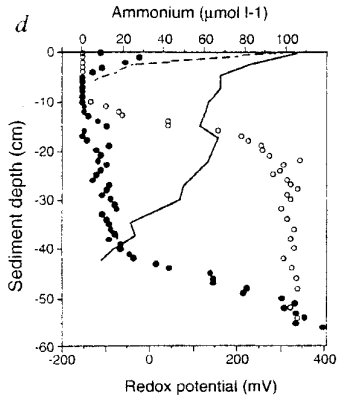

Figure 5.11 Redox (solid line) and NH_4^+ profiles (filled circles) in sediment inhabited and uninhabited (dotted line and open circles) sediment, taken from Ziebis et al. (1996).

Having found a P_{DOC} value that produced the required NH_4^+ levels in the absence of burrows, I had planned to substitute this value directly into the oscillating irrigation (radial) model, using burrow radii inferred from the resin casts and population density. To fit the oscillating model to the data, irrigation parameters would need to be found that produce an oxygen penetration depth of 3mm at burrow oxygen levels of 17% and 38% of air saturation. The oscillating model is very time-consuming to run, and it is best used to infer the burrow concentrations using known irrigation parameters. In this case we do not know the irrigation behaviour, but we do know the burrow concentrations for two important species: O_2 and NH_4^+. A further complication is that the burrow oxygen records (particular at 26cm depth) show dramatic changes in oxygen levels over a very short space of time (eg a drop from 43% to 17% in the space of minutes, Figure 5.12).

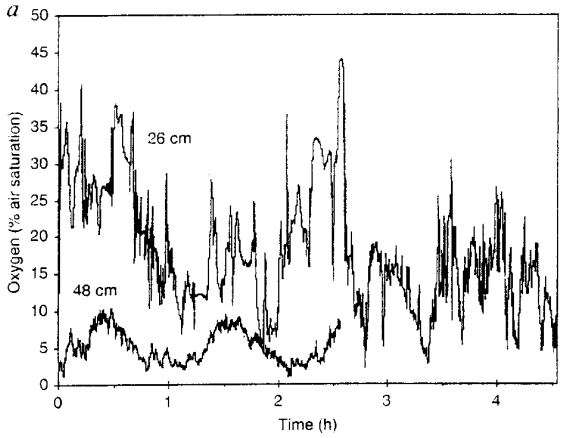

Figure 5.12 Continuous oxygen measurements within a burrow at 26 cm and 48 cm depth, taken from Ziebis et al. (1996).

This kind of behaviour cannot be reproduced in the model; the sediment oxygen demand would need to be extremely high to produce such rapid drops in oxygen, yet this would then be incompatible with the measured oxygen penetration depths. The most likely cause of the rapid changes in burrow oxygen levels is that water of varying oxygen concentrations was advected along the burrow lumen. For these reasons constant, partially flushed conditions were assumed within the burrow. As the flushing rate increases, the burrow oxygen level increases and the burrow NH_4^+ level decreases. By running the model for a range of flushing rates, I was able to select rates that provided a good match to measured burrow oxygen levels (eg. Figure 5.13). The burrow geometry settings were r_1 = 0.2cm and r_2 = 5cm (derived from the population density of 120 individuals/m², $120\pi r_2^2 = 10^4 \text{cm}^2$).

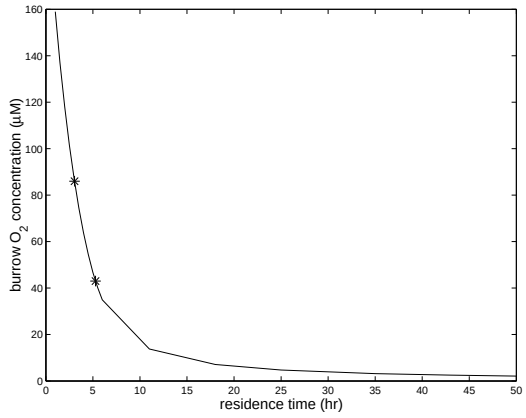

Figure 5.13 Modelled burrow oxygen concentrations as a function of burrow flushing rates (represented here as burrow residence time). Asterisks mark the measured oxygen concentrations in *Callianassa truncata* burrows at depths of 20cm and 40cm below the sediment surface.

Using the above parameters, the predicted oxygen penetration distances from the burrow wall, 7 mm and 10 mm, were greater than the measured values, both 3 mm, and the modelled NH_4^+ levels 3-4 cm from the burrow, >50 µmol/L, were much higher than the measured values at that distance, < 15 µmol/L. These results present a seemingly irresolvable situation. Either increasing the P_{DOC} value, or decreasing the burrow flushing rate, would decrease the oxygen penetration distance, however both these alterations to the model would increase the porewater NH_4^+ concentrations. The modelled NH_4^+ concentrations are already much higher than the measured values, and so a further increase would only worsen the match between modelled and measured data.

Further runs were conducted experimenting with the radial distribution of P_{DOC}. It is widely believed that burrow walls have a higher mineralisation rate than the surrounding sediment. In earlier chapters we saw that burrows can function to subduct surface material to considerable depths where it can be incorporated into the burrow wall. Mucus linings needed to maintain burrow structural integrity can also be a source of organic matter. Kristensen (2000) suggested a higher mineralisation rate at the burrow wall could be due to old, partly degraded organic matter being exposed to oxygen (estimated to increase the mineralisation rate by a factor of ten). Other suggestions include microbial stimulation by grazing and oscillating redox conditions (Aller (1994)).

While the precise mechanisms remain unclear, there appears to be wide consensus that enhanced mineralisation is likely to occur at the burrow wall. To test the effect of this in model I altered the P_{DOC} term to be a step function, with a higher value within a band of sediment immediately surrounding the burrow (the region $r_1 \le r < r_w$):

$$P_{\mathrm{DOC}} = \begin{cases} P_1 = f_c P_2 & r_1 \le r < r_w \\ P_2 & r_w \le r \le r_2 \end{cases} \qquad \textbf{(5.22)}$$

where f_c is simply a prescribed factor. To allow direct comparison with the uniformly distributed P_{DOC} case, $P_{\mathrm{DOC}} = P_c$ (uniformly distributed between r_1 and r_2), P_1 and P_2 were set so that the total mineralisation rate (obtained by integrated between r_1 and r_2) was the same in each case. This requirement sets P_2 to be:

$$P_2 = \frac{P_c\left(r_2^2 - r_1^2\right)}{f_c\left(r_w^2 - r_1^2\right) + \left(r_2^2 - r_w^2\right)} \qquad \textbf{(5.23)}$$

Model runs were repeated with altered P_{DOC} distributions as specified in equations (5.22) and (5.23). Values of f_c = 10 and f_c = 100 were tested. The region of enhanced mineralisation was set to be a 3mm band of sediment immediately surrounding the burrow. Comparisons for all three model runs are presented in Figure 5.14 and Figure 5.15.

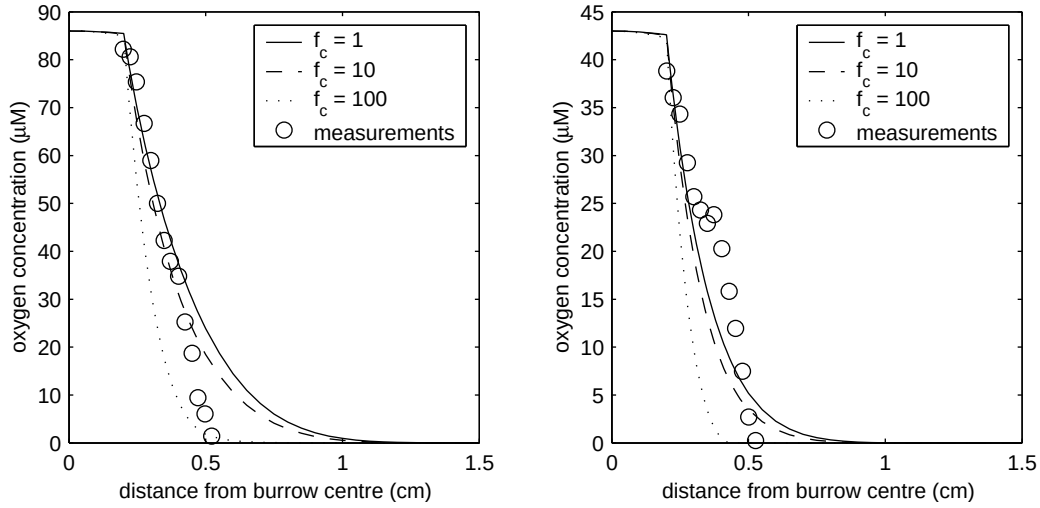

Figure 5.14 Modelled and measured oxygen profiles radiating from burrow tubes. Measurements taken at 20cm depth (left) and 40cm depth (right) (Ziebis et al. (1996)).

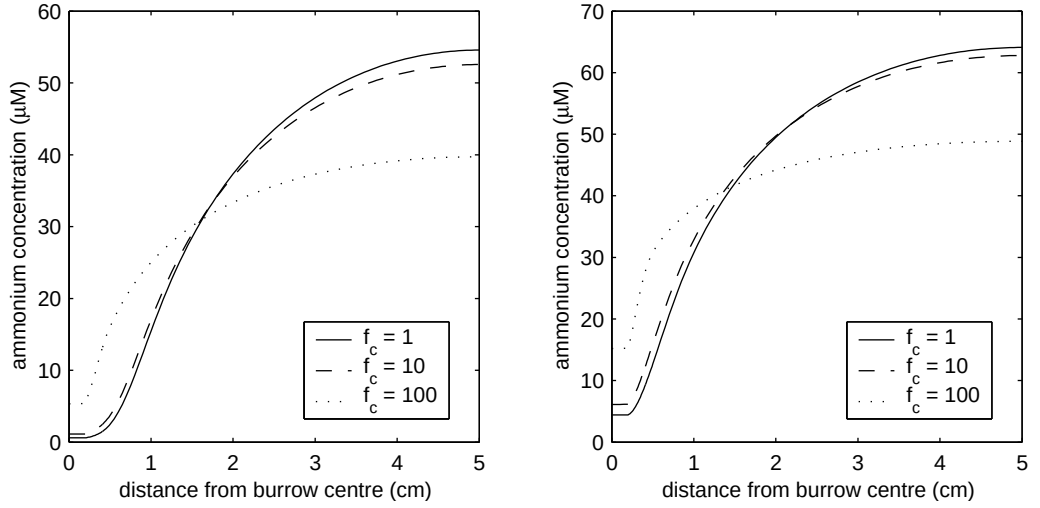

Figure 5.15 Modelled NH_4^+ profiles radiating from burrow tubes. The two scenarios represent the 20cm depth (left) and 40cm depth (right) simulations.

Three differences to the measurements are obvious. Firstly, in all model runs the oxygen profiles were markedly different in shape to those measured by Ziebis et al. (1996). The modelled oxygen profile shapes were typical of exponential decline with distance, but measured tube profiles were roughly linear. Secondly, the measurements suggest that oxygen penetration distance is roughly 3 mm, regardless of the burrow oxygen concentration, yet the model always predicts deeper oxygen penetration associated with higher burrow oxygen levels. Thirdly, in all model runs, the NH_4^+ concentrations away from the burrow far exceed the measured values, although the modelled burrow NH_4^+ concentrations fall within the range of measured field values.

The model results only come close to matching the oxygen penetration distance and far-field NH_4^+ concentrations when the rate of DOC production in the burrow wall exceeds the rate in the surrounding sediment by a factor of 100.

Clearly there is no one elegant model configuration which explains all the data. My inability to match both NH_4^+ data and O_2 data simultaneously highlights the fact that the model is a serious simplification of reality, and does not capture the full complexity of the field processes. Likely explanations include:

1. advection: the sediment is highly permeable, so diffusion and reaction may not be the only processes influencing concentration distributions. Complicated advection patterns may dramatically alter porewater distributions (Huettel and Webster (2001)). In the lower sections of the burrow (>10 cm from the sediment surface) the burrow is basically a single shaft, and not a tube connecting two surface openings. Conservation of volume may require that the fluid the shrimp displaces as it wanders along such a shaft is forced through the permeable wall into the surrounding sediment, hence the mere act of roaming its burrow may induce a transitory pumping effect in the near vicinity of the burrow.

2. sediment sorting: Ziebis et al. (1996) described preferential ejection of fine material and incorporation of larger grains into chamber walls, so it is likely that sediment packing is substantially altered at the burrow wall. Changes to sediment packing alter the tortuosity, and so the porewater diffusion coefficient of dissolved species.

3. time-varying system: the history of the concentration distributions and transport processes is unknown, yet could significantly impact on the measured distributions. The field system was almost certainly not at steady state. I ran the model for 2 months, starting from an assumption of uniformly mixed sediment, and this was insufficient to reach steady state conditions. The authors took measurements 2 months after observatory installation, and the extent of mixing due to installation is unknown.

4. reaction kinetics: the model assumes first order reaction kinetics for oxygen consumption when oxygen levels are below 30 μmol/L and zeroth order kinetics for oxygen concentrations greater than this. The profile shape emerging from the combination of species reaction and diffusive transport vary with the type of

reaction kinetics. The exponential decay shape is typical of first order reactions. If the value of C_{crit} is altered in equation (5.8) different shaped profiles will result.

Later sections of this chapter investigate the impact of burrow irrigation on nitrification and denitrification rates, as it has been widely suggested that irrigated burrows can increase both these rates. For this reason I calculated the nitrification and denitrification rates associated with the above model runs, and present them in Table 5.2 for completeness.

Table 5.2 Denitrification efficiencies and denitrification:nitrification ratios for *C. truncata* model runs.

Scenario	Denit efficiency (at 2 months)	Denit/Nit (at 2 months)	Denit efficiency (Steady state)	Denit/nit (Steady state)
20 cm depth, f_c =1	0.55	0.74	0.60	0.64
20 cm depth, f_c =10	0.52	0.71	0.62	0.65
20 cm depth, f_c =100	0.41	0.73	0.52	0.71
40 cm depth, f_c =1	0.44	0.73	0.47	0.63
40 cm depth, f_c =10	0.45	0.75	0.52	0.69
40 cm depth, f_c =100	0.34	0.78	0.47	0.77

5.5.2 Case 2: modelling *Callianassa subterranea* laboratory data (Forster and Graf (1995))

Forster and Graf (1995) measured irrigation currents and oxygen levels in *C. subterranea* burrows. The specimens were taken from silty fine sand in the North Sea and housed in flat aquaria (50cm x 40cm x 5cm) where burrow development, oxygen levels and irrigation velocities could be measured.

When compared to the *C. truncata* study, a very different picture emerges. Only the upper sections of *C. subterranea* burrows were studied (oxygen measurements were made no deeper than 17 cm below the sediment surface), whereas Ziebis et al. (1996) report only oxygen measurements made at depths greater than 20 cm from the surface. At these depths *C. truncata* burrows contained significant oxygen concentrations; by contrast, for most of the time there was no detectable oxygen in *C. subterranea* burrows 17 cm from the surface. Oxygen penetration distances into the surrounding sediment were typically 3 and 7 mm for *C. trunctata*, yet Forster and Graf (1995) reported that oxygen penetration was less than 0.25 mm into the surrounding sediment at 170mm from the surface, and around 1mm at 16mm from the surface.

Forster and Graf (1995) described two forms of burrow irrigation: regular and irregular. Regular irrigation was characterised by quiescent periods lasting 40 minutes interspersed with brief irrigation periods lasting 150 seconds. Irregular irrigation occurred when the animal was observed rushing rapidly around the upper sections of the burrow. Irregular irrigation events lasted less than a minute, but the flow velocity could be substantially higher than the regular irrigation flow velocity (up to 2 cm/s for irregular irrigation, 0.3 cm/s for regular irrigation). Oxygen measurements at 17cm below the sediment surface suggest that oxygen is only present in this section of the burrow during periods of irregular irrigation.

The study described burrow geometry, irrigation behaviour and oxygen measurements, and so there ought to be sufficient information to parameterise the model. In particular, the measurements taken in the upper section of the burrow seem conducive to modelling as there are simultaneous irrigation and oxygen data. Away from any burrows, the oxygen penetration distance was 4 mm from the sediment surface. A vertical version of the nitrogen model was used to determine the value of P_{DOC} that produces this penetration distance, and this was P_{DOC} = 400 μmol/L/d. This same value was then substituted into a radial version of the model, with r_1 set at 0.3 cm and r_2 = 2.5cm. The animals were burrowing in aquaria that were 5 cm thick, which places a constraint on the size of r_2. The value of r_1 simply followed from the authors' measurements of burrow diameters. The irrigation parameters were set up so that the irrigation frequency was 40 minutes, the irrigation duration was 150 seconds, again the measured values. Forster and Graf (1995) measured oxygen levels 16 mm from the sediment surface and 1mm from the burrow wall within the sediment surface. During irrigation periods they measured oxygen levels of 80% saturation, which then dropped at a rate of 25.2 μmol/L/min (quoted as 0.42 nmol O_2 /cm^3/s in the paper).

Matching model results to measurements again proved to be difficult. Firstly, the authors reported an instantaneous large rise in oxygen levels (0% to 80% saturation) 1mm from the burrow wall within the sediment (Figure 5.16).

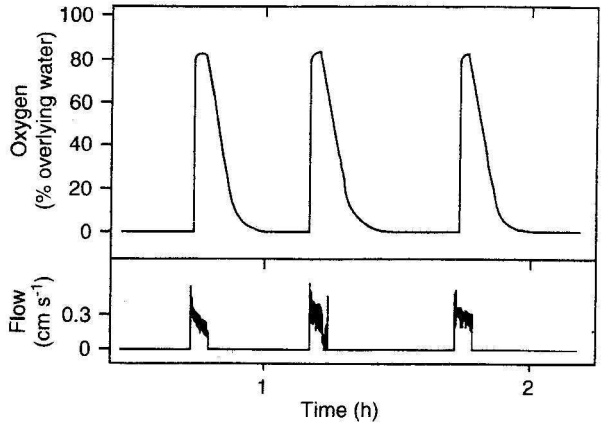

Figure 5.16 Changes in oxygen concentration (measured by an oxygen sensor position 1mm from burrow wall, within the sediment) registered with simultaneous measurements of flow above the "inhalant" funnel opening, taken from Forster and Graf (1995).

Diffusion through the sediment is a slow process, even across a distance of only 1mm. To illustrate the point, we can make the generous assumption that oxygen is diffusing through water (no sediment) and it is not being consumed by any reactions. Initial conditions are zero oxygen at all locations and for $t > 0$ the concentration at $x = 0$ is C_o. Further assumptions include a no flux boundary at a distance L and cartesian, rather than radial, coordinates have been used for simplicity. The governing equations are:

$$\frac{\partial C}{\partial t} = D\frac{\partial^2 C}{\partial x^2} \qquad \textbf{(5.24)}$$
$$C(x,0) = 0$$
$$C(0,t) = C_0$$
$$\frac{\partial C}{\partial x}(L,t) = 0$$

and the solution is (Boudreau (1997)):

$$C = C_0 + \sum_{n=1}^{\infty} -\frac{2C_0}{L\beta_n}\sin(\beta_n x)\exp\left(-D\beta_n^2 t\right) \qquad \textbf{(5.25)}$$
$$\beta_n = \frac{(n-1/2)\pi}{L}$$

Assuming L = 1 cm (an arbitrary choice, set to be sufficiently far away from the oxygen penetration distance) and D = 1.8 cm²/d the concentration will reach $C = 0.8C_0$ at x = 0.1 cm when $t \sim 60$ minutes. In the scenario described by Forster and Graf (1995) the time required would be even longer as the oxygen is diffusing through sediment and it

is being consumed by reactions in the sediment. Without knowing further details about the experimental setup, it could be possible that the sensor placement induced some additional transport, so burrow water was advected to the sensor location during burrow irrigation periods. If this is so, the oxygen time series is maybe more representative of oxygen levels within the burrow, at the burrow wall. Unfortunately, this too seems unlikely. The rate of oxygen depletion once irrigation has stopped is remarkably high. Unlike in the *C. truncata* study, where we could speculate that along-burrow advection currents could rapidly transport patches of oxygen depleted water past the oxygen sensor, thus explaining the large, rapid changes in oxygen levels, Forster and Graf (1995) reported simultaneous velocity measurements which confirm that the burrow water was quiescent. If oxygen levels are at 80% saturation at the burrow wall, the model can only explain such a rapid drop to 0% saturation if mineralisation rates in the surrounding sediment are extremely high. This possibility is excluded by the fact that the modelled oxygen distribution would penetrate a much smaller distance than the measured 1 mm penetration distance in the burrow wall and ~4mm at the sediment surface. The vertical model suggested that the P_{DOC} needs to be around 400 µmol/L/d to produce a 4mm oxygen penetration at the surface.

As an aside, I did find a model configuration that produced a reasonable match to the time-series given by Forster and Graf (1995) (Figure 5.17). It was a spherical model with small values of r_1 (0.5mm) and r_2 (4mm), and all other parameters were kept unchanged (P_{DOC} = 400 µmol/L/d; 150s irrigation period in each 40 minute irrigation cycle). This model was constructed to test the following scenario: during burrow irrigation, burrow water is advected to the sensor tip embedded in the sediment so triggering an instantaneous rise in the oxygen time series; once irrigation stops the tip is surrounded by oxygen consuming sediment and the oxygen at the sensor tip is rapidly depleted (Figure 5.18). The spherical model result in Figure 5.17 lends credibility to this possibility.

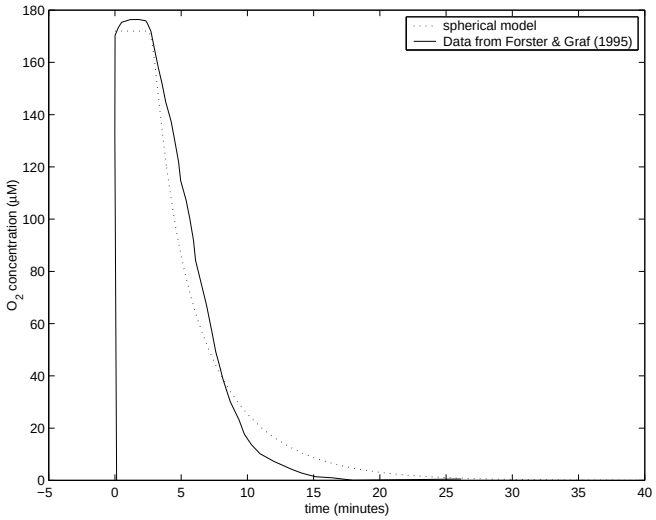

Figure 5.17 Oxygen data from Figure 5.16 (assuming the O_2 concentration in the overlying water is 215 µmol/L) compared with spherical model result (see text for details.)

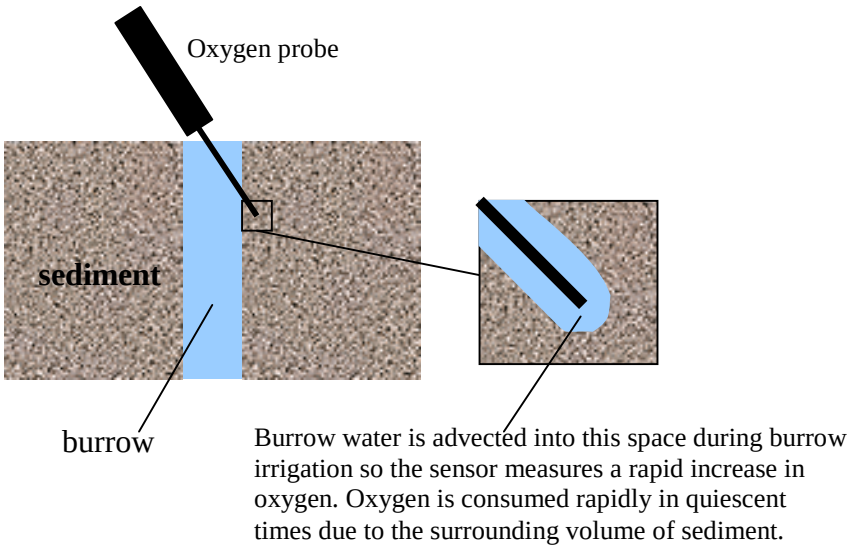

Figure 5.18 Possible explanation for high rate of oxygen increase and decline measured by Forster and Graf (1995) 1mm from burrow wall.

A conflict remains: assuming P_{DOC} = 400 μmol/L/d, there should still be some oxygen present 1mm from the burrow wall, yet the measurements suggest it is anoxic for the majority of the time. This characteristic of the data is curious, and conflicts with standard expectations. For example, Fenchel (1996) measured oxygen penetration depths at the sediment surface and in the sediment surrounding worm burrows. He found that the measurements matched well with a theoretically derived relationship between the sediment and burrow oxygen penetration depths:

$$L_b = -r_1 + \sqrt{r_1^2 + 2r_1 L_s} \qquad \textbf{(5.26)}$$

where L_b and L_s are the oxygen penetration distances at the burrow wall and sediment surface respectively. Using this relationship and assuming r_1 = 3 mm and L_s = 4 mm, equation (5.26) predicts a burrow oxygen penetration distance of 2.7 mm (compared to <1mm measured). The derivation of (5.26) did not include confounding influences such as differing diffusive boundary layer thicknesses between burrow and the surface, and it assumed the same oxygen concentration in the burrow and at the surface. Yet Fenchel (1996) found that measurements from worm burrows matched the theoretical estimates very well.

Another possible explanation for the unexpectedly low burrow oxygen penetration is that the burrow wall is lined with material with a dramatically different mineralisation rate to the surface sediment (and consumes all the oxygen within 1mm from the burrow). I used the model to investigate both a homogeneous and heterogeneous P_{DOC} distribution:

Case 1: Used a uniform value of P_{DOC} = 400 μmol/L/d (obtained from matching oxygen penetration distances at the surface).

Case 2: Assumed there is a 2 mm band surrounding the burrow with a higher P_{DOC} value (details in Table 5.3).

The oxygen time series data and corresponding flow meter measurements provide good information about the irrigation behaviour, so supplying well-constrained irrigation parameters that can be used in both cases. The results for the two cases are listed in Table 5.3.

Table 5.3 Model results simulating two laboratory scenarios and a field scenario.

	Case 1	Case 2	Field case
P_{DOC} (μmol/L/d)	400	$\begin{cases} 10000 & r_1 \le r < r_1 + 2\text{mm} \\ 400 & r_1 + 2\text{mm} \le r \le r_2 \end{cases}$	2500
Oxygen penetration depth (mm)	4	1.5	1
Oxygen flux per unit burrow length (μmol O_2 cm^{-1} day^{-1})	1.7	2.8	3.1
Nitrification rate (per unit burrow length) (μmol N cm^{-1} day^{-1})	683	339	1184
Denitrification rate (per unit burrow length) (μmol N cm^{-1} day^{-1})	402	218	562
Denitrification efficiency	0.43	0.14	0.1
Denitrification : nitrification	0.59	0.64	0.47

Burrow measurements made by Forster and Graf (1995) 17cm from the sediment surface recorded zero oxygen levels during regular irrigation events. Regular irrigation pumped overlying water into the burrow at a rate of 6 mL h^{-1}. The oxygen concentration of the overlying water in the laboratory was 215 μmol L^{-1}. For the oxygen to be zero in the burrow at a distance of 17cm from the burrow opening, all the oxygen must have been consumed by the walls. These measurements suggest a per unit burrow length oxygen consumption rate of at least 1.8 μmol O_2 cm^{-1} day^{-1} in the upper 170 mm of the burrow. Case 1 predicts this oxygen flux well (1.7 μmol O_2 cm^{-1} day^{-1}). Case 2 overestimates the flux (2.8 μmol O_2 cm^{-1} day^{-1}), however this result is not necessarily inconsistent with the inferred flux of 1.8 μmol O_2 cm^{-1} day^{-1}, as this is minimum flux that is necessary to consume all the oxygen in the upper 17cm of the burrow. Nitrification and denitrification rates are substantially higher for Case 1, demonstrating the significant influence mineralisation rates (and distribution) can have on the nitrogen dynamics.

These model runs simulated the laboratory conditions. Forster and Graf (1995) also measured oxygen profiles *in situ*. The oxygen gradient at the surface was much steeper, suggesting a higher sediment mineralisation rate in the field. In addition, the oxygen concentration in the overlying water was markedly different (presumably due to different temperatures). The field oxygen concentration was 292 μmol/L, whereas the oxygen concentration in the laboratory water was around 215 μmol/L.

Assuming that the irrigation behaviour remains the same as in the laboratory, the impact of this behaviour on the field sediments can be assessed using the model. As before, the P_{DOC} value was found by matching the oxygen penetration distance measured at the sediment surface (2.5 mm), yielding a value of P_{DOC} ~ 2500 μmol/L/d. The results are listed in Table 5.3. The per unit burrow length oxygen consumption rate was 3.1 μmol O_2 cm^{-1} day^{-1}, which is substantially higher than the above estimate of 1.8 μmol O_2 cm^{-1} day^{-1}. If, as the authors suggested, oxygen is advected into the burrow at a rate of 1.75 μmol O_2 cm^{-1} day^{-1}, then at this rate of burrow wall oxygen consumption the oxygen would be completely consumed within 13.5cm of the burrow opening (compared to 17 cm in the laboratory).

It is conceivable that the shrimp matches its behaviour to the surrounding sediment conditions. Given the higher sediment oxygen consumption rates in the field sediments, it would not be surprising to find that the shrimp increases its burrow irrigation rate accordingly.

5.5.3 Case 3: modelling *Callianassa japonica* and *Upogebia major* laboratory measurements (Koike and Mukai (1983))

Koike and Mukai (1983) measured oxygen, nitrate plus nitrite and NH_4^+ concentrations in burrows in laboratory aquaria occupied by *Callianassa japonica* and *Upogebia major*. These measurements were made with constant overlying water conditions (water temperature 20.5°C), and further oxygen measurements were taken during periods of simulated low tide, where the overlying water level was lowered to become level with the sediment surface. The authors inferred burrow irrigation rates using an oxygen mass balance. The authors also measured individual shrimp respiration rates.

The radial nitrogen model developed here was used to simulate the two scenarios (high tide and low tide) described in the experiments. No measurements of burrow radius were provided by Koike and Mukai (1983), although typical callianassid burrow radii range from 0.2 – 0.5 cm. The authors stated that the natural population density is ~ 20 individuals m^{-2}, which corresponds to r_2 = 12.6 cm. However, the laboratory aquaria were only 3 cm wide, so limiting the size of r_2 to 1.5 cm.

5.5.3.1 High tide

During high tide conditions the shrimp can maintain a flow through their burrow, frequently flushing the burrow with overlying water. Koike and Mukai (1983) did not

investigate the irrigation behaviour, however they did infer irrigation rates from their measurements. Their oxygen measurements were only taken every 30 minutes, too low a sampling frequency to infer the irrigation patterns. The oxygen measurements, burrow volumes and irrigation rates were used to infer the irrigation parameters required in the model. The value of f in equation (5.11) was estimated by assuming that the maximum and minimum oxygen concentrations represent the burrow concentrations during irrigation and at the end of quiescent periods, respectively.

The calculation for *C. japonica* is:

$$C = fC_o + (1-f)C_q \qquad \textbf{(5.27)}$$
$$\Rightarrow 0.45C_0 = fC_o + 0.12C_0(1-f)$$
$$\Rightarrow f = 0.37$$

and for *U. major*:

$$C = fC_o + (1-f)C_q \qquad \textbf{(5.28)}$$
$$\Rightarrow 0.41C_0 = fC_o + 0.3C_0(1-f)$$
$$\Rightarrow f = 0.16$$

The model also requires the length of irrigation period (T_i) which can be estimated from f, the burrow volume (V_b) and the irrigation rate (Q_b):

$$T_i = \frac{fV_b}{Q_b} \qquad \textbf{(5.29)}$$

Making these assumptions irrigation periods of 20 minutes for *C. japonica* and 18 minutes for *U. major* were estimated. A further assumption was made that the shrimp only actively pumped water through their burrow for 5% of the irrigation period, based on irrigation behaviour measured in Forster and Graf (1995).

The respiration rates for both species were measured at full oxygen saturation, yet it is likely that the respiration rate is a function of the ambient oxygen concentration. This effect was studied in detail by Paterson and Thorne (1995) for *Trypaea australiensis*. They found that respiration reduced with lower oxygen concentrations, and shut down completely below a critical oxygen concentration. Their findings were applied to the model here, assuming the same shape for the respiration vs oxygen concentration relationship. Koike and Mukai (1983) also commented that they observed a decrease in respiration rate at lower oxygen concentrations.

Koike and Mukai (1983) conducted their experiment 4 to 5 days after burrow construction, and so the model was run for 5 days. The model was also run for 20 days, with negligible differences in the results. A series of model runs were conducted testing changes to burrow radius, irrigation behaviour (*f*) and porosity to assess the model parameters that would bring the model into reasonable agreement with measurements. Each run spanned a range of P_{DOC} values (200 – 1200 μmol L^{-1} d^{-1}). The results given in Figure 5.19 used the following parameter values: P_{DOC} = 700 μmol L^{-1} d^{-1}; r_1 = 0.4 cm; ϕ = 0.4; f = 0.2 (*C. japonica)* and f = 0.16 (*U. major*). In both cases oxygen is well matched and NO_3^- levels are overestimated (by up to a factor of 4.5). The extremes of the NH_4^+ range are poorly predicted, although the modelled values fall within the measured range.

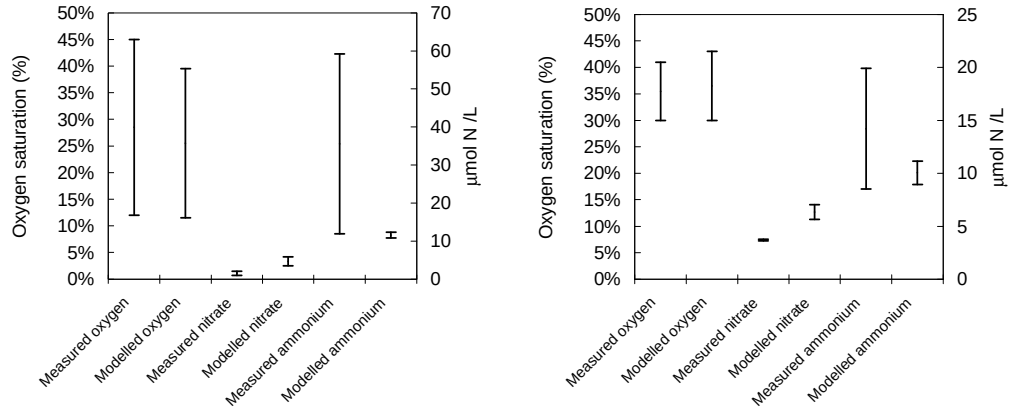

Figure 5.19 Measured and modelled burrow O_2, NO_3^- and NH_4^+ concentration ranges for *Callianassa japonica* (left) and *Upogebia major* (right). Measured values are from Koike and Mukai (1983).

The difficulty in finding a better match lies with the fact that measured NO_3^- levels were low, despite the presence of significant levels of NH_4^+ in an oxygenated environment. The difficulties faced in attempting to model this scenario are a direct contrast to those experienced when attempting to model the *Callianassa truncata* data, where measured NH_4^+ levels were much lower than could be explained by the model. A possible model modification that may account for the very low NO_3^- levels is a substantial increase in the rate constant for denitrification, k_4. Following Blackburn and Blackburn (1993), this value has been set at 30 day^{-1}, however other papers by the same authors have used significantly different values. Blackburn (1996) used a value of k_6 = 500 day^{-1} and Blackburn et al. (1994) employed k_4 = 5000 day^{-1}. An extraordinary range of values (spanning two orders of magnitude) has been used with the justification of

creating a better fit to measurements. The higher rates imply a very dense and large biomass of denitrifying bacteria (Blackburn et al. (1994)). I tested the effect of a more extreme value. Increasing k_4 to a value of 1000 day^{-1} brought the modelled NO_3^- levels closer to the measured range (at most a factor of 2.6 too high, Figure 5.20).

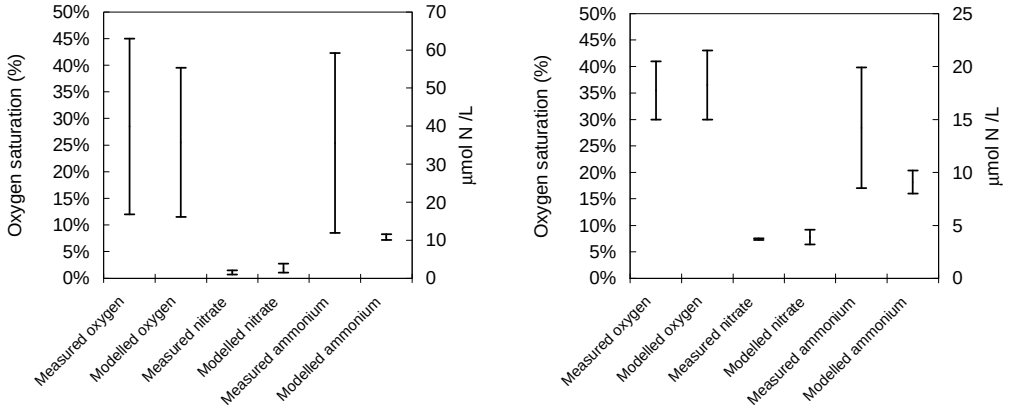

Figure 5.20 Measured and modelled burrow O_2, NO_3^- and NH_4^+ concentration ranges for *Callianassa japonica* (left) and *Upogebia major* (right). Same model parameters as Figure 5.19, except k_4 = 1000 day^{-1}. Measured values are from Koike and Mukai (1983).

The model results were quite insensitive to the massive increase in k_4, with the only real effect being a reduction in NO_3^- levels (to roughly half their previous values). The nitrification and denitrification rates for both scenarios are shown in Table 5.4. As expected, the denitrification rates are higher in the second scenario (where k_4 = 1000 day^{-1}), although the rates (and efficiencies) have increased by no more than 50% despite the large increase in k_4.

Table 5.4 Model nitrification and denitrification behaviour under two k_4 values.

	Nitrification rate (nmol/cm/day)	Denitrification rate (nmol/cm/day)	Denitrification :nitrification	Denitrification efficiency (%)
C. japonica (k_4 = 30 day^{-1})	91.8	53.4	58%	29%
C. japonica (k_4 = 1000 day^{-1})	99.4	79.9	80%	43%
U. major (k_4 = 30 day^{-1})	117.7	71.5	61%	39%
U. major (k_4 = 1000 day^{-1})	126.3	99.8	79%	54%

These rates are expressed as rates per unit burrow length, and so the length of burrow beneath each m^2 of surface sediment is needed to convert these rates to an areal estimate. At first glance, this appears to be a simple matter of multiplying the rates by the average burrow length and the areal density of burrows. At this point, however, it

becomes clear that the experimental configuration may have created burrow conditions which are not representative of natural conditions.

As mentioned earlier, the natural density of these shrimp *in situ* is approximately 20 individuals m^{-2}, which corresponds to a value of r_2 = 12.6 cm. The laboratory tank was only 3 cm wide, so limiting r_2 to a smaller value. A value of r_2 = 1.5 cm was used in the model, which represents a lower bound on this distance. The distance determines the potential accumulation of NH_4^+ in the sediment. For large values of r_2, relatively little of the NH_4^+ being produced will diffuse to oxygenated burrow walls and so it will accumulate within the sediment. For small values of r_2, there is a lot of oxygenated burrow area beneath the sediment and so more of the NH_4^+ will diffuse into these areas, where it can be transformed through nitrification. The eventual NH_4^+ concentrations, and the amount of NH_4^+ oxidised to NO_3^-, is most critically determined by the burrow spacing.

The model was run again for 20 days, setting r_2 = 12 cm. As expected, this simple alteration produced a significant difference in the results (Figure 5.21). Most notably, the predicted NO_3^- and NH_4^+ levels were larger than measured values. This effect would be further increased if the model run time had been extended, as the system had still not reached steady state after 20 days.

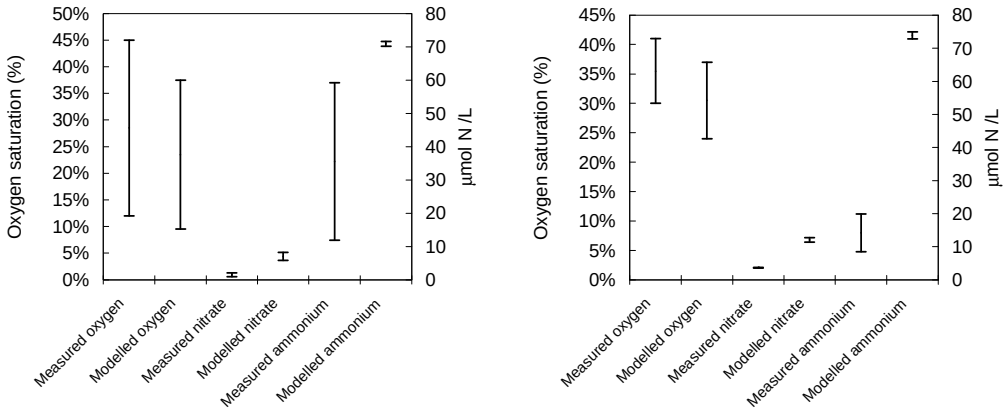

Figure 5.21 Measured and modelled burrow O_2, NO_3^- and NH_4^+ concentration ranges for *Callianassa japonica* (left) and *Upogebia major* (right). The model has been modified to set r_2 = 12 cm. Measured values are from Koike and Mukai (1983).

The predicted nitrification and denitrification rates are roughly double the rates predicted in the smaller-radius cases (Table 5.5). The proportion of NO_3^- being

denitrified reduced by a small amount (from ~80% to ~60%), but the denitrification efficiency has dropped substantially (from ~45% to 1%).

Table 5.5 Model nitrification and denitrification results when r_2 = 12 cm.

	Nitrification rate (nmol/cm/day)	Denitrification rate (nmol/cm/day)	Denitrification :nitrification	Denitrification efficiency
C. japonica (k_4 = 1000 day^{-1})	263.67	153.12	58%	1%
U. major (k_4 = 1000 day^{-1})	339.58	193.87	57%	1%

In the absence of information on the burrow locations and density within the tank, the choice of an appropriate r_2 value is difficult. Certainly the 'correct' value will be somewhere between 1.5 cm and 12 cm. We can infer from the results of these two extremes that NO_3^- levels will be generally over-estimated by the model. NH_4^+ levels fall within the measured range, however the extent of the range was not predicted.

The importance of r_2 makes interpretation of the laboratory experiments difficult. I found a model configuration that provided a reasonable approximation to the laboratory measurements. It may be valid simply to increase the value of r_2 to the field value and infer the new burrow concentrations and rates. This would assume, however, that the shrimp behaves in the same manner, regardless of the surrounding chemistry. A more likely scenario is that a shrimp will respond to its surroundings and will alter its irrigation pattern to create a burrow environment best suited to its needs. These considerations make it difficult to estimate the likely nitrification and denitrification rates.

5.5.3.2 Low tide

During the low tide simulation, Koike and Mukai (1983) noted a rapid drop in *Upogebia major* burrow oxygen levels (54% to 16% saturation within one hour) followed by a relatively constant oxygen concentration for the remaining 4 hours (Figure 5.22). These observations proved difficult to reproduce in my model. In the absence of a respiring shrimp, the burrow walls would still have been consuming oxygen at a considerable rate, making it difficult to explain a constant oxygen concentration persisting (and even increasing slightly at one point) for a period of several hours. The authors suggested that oxygen continued to be supplied to the burrow during low tide: they observed the shrimp showing frequent irrigation motions while occupying the upper portions of the burrow. It is not clear that such activity would markedly increase the supply of oxygen

to the burrow water. There is no capacity for the shrimp to produce a continuous flow through its burrow because the water level is reduced to the sediment level, so oxygen would have to diffuse across the air-water interface at the burrow opening.

There are two possible explanations for the relatively constant oxygen levels. Shrimp respiration may shut down completely at a relatively high value; in previous runs it was assumed that shrimp respiration ceases at 6 μmol L^{-1} O_2, based on the results published by Paterson and Thorne (1995). The second possibility is that oxygen was injected into the burrow during measurements. Each oxygen measurement required the withdrawal of approximately 12-16mL of water from the burrow which was circulated past an oxygen sensor and re-injected into a different section of the burrow. The volume of the external system was 3.5 mL, which represented approximately 8% of the burrow volume. It is possible that the water residing in the external system became oxygenated between measurements (taken every 30 minutes), and this partially oxygenated water would then have been injected into the burrow at the start of each measurement.

Three model scenarios were run:

Case 1: Model parameters the same as in previous section (with r_2 = 1.5 cm, k_4 = 1000 day^{-1});

Case 2: Same as Case1, with shrimp respiration altered to shut down at 35 μmol L^{-1}.

Case 3: Same as Case 2, with oxygen injection at each measurement (assumed that 8% of the burrow is replaced with oxygen at 60% saturation).

The results, plotted in Figure 5.22, show that Case 3 gives the closest match to measured data. The Case 2 results demonstrate clearly that in the absence of shrimp respiration the oxygen levels are still expected to decline significantly as a result of oxygen consumption by the surrounding sediment. Only a continuing supply of oxygen can ensure the maintenance of a steady oxygen concentration over a period of hours. Case 3 demonstrates that if the external volume of 3.5 mL were oxygenated to 60% and injected into the burrow, this would be sufficient to keep oxygen measurements reasonably constant. Note, however, that Case 3 still requires respiration to be shut down at 35 μmol L^{-1} O_2.

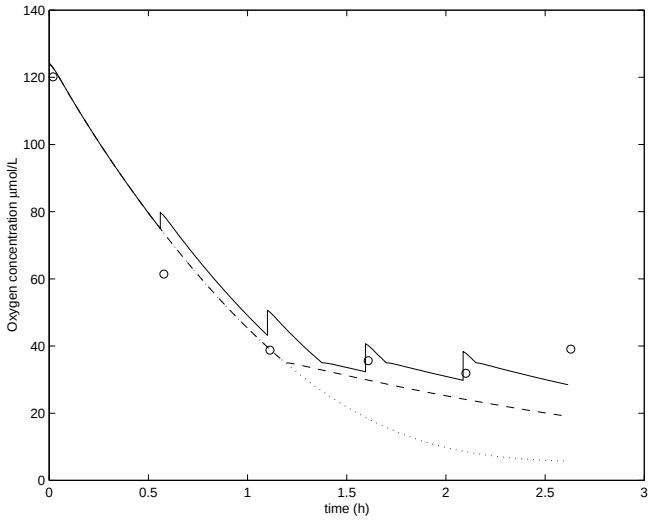

Figure 5.22 Oxygen concentration in the burrows of *Upogebia major* under simulated low tide condition. Circular markers are data points taken from Koike and Mukai (1983). The lines are the three model scenarios (Case 1, dotted; Case 2, dashed; Case 3, solid).

5.5.4 Summary of thalassinidean shrimp cases

Despite the availability of good experimental and field data on thalassinidean burrow chemistry, and the existence of well-accepted models of sediment nitrogen dynamics, the preliminary attempt here to combine this knowledge created as many problems as it solved. This experience reinforced the oft-repeated advice that experimentalists and modellers should work together. Given that the experiments considered here were conducted in the absence of any prior knowledge about within-burrow concentrations, they provided an excellent starting point by providing a snapshot of concentration distributions in burrows. These snapshots, however, were insufficient to resolve modelling questions. More will be gleaned from future experiments if they are conducted with an explicit theoretical framework underlying the design, with the aim of integration with modelling work.

Methodological considerations were highlighted, particularly in regard to laboratory measurements. For example, it may be insufficient to have the shrimp inhabiting their native sediment if some attempt is not made to recreate the sediment geometry and organic matter distribution if meaningful estimates of *in situ* burrow chemistry are sought. In particular, if an animal usually has a 10cm wide annulus of sediment surrounding its burrow, this should be recreated in the laboratory if the aim is to measure burrow chemistry.

Attempts to model *Callianassa japonica* and *Upogebia major* measurements were more successful than attempts to model *Callianassa truncata* and *Callianassa subterranea* measurements. This was largely attributable to the fact that data on three of the chemical species of interest, oxygen, NO_3^- and NH_4^+, were available, and the authors had measured individual shrimp respiration rates.

This work raised several questions in need of answers, including:

1. What are the solute transport processes within the burrow and within the surrounding sediment? Diffusive transport assumptions were not able to explain the sediment oxygen data by Forster and Graf (1995). Advective flows through the sediment may be important in the system studied by Ziebis et al. (1996).

2. What is the sediment respiration rate, and how is it spatially distributed within the sediment? Experiments could include measuring respiration rates from cores of differing length, and repeating the experiments with uniformly-mixed sediment cores of differing length. Work along similar lines by Aller and Aller (1998) yielded very surprising results. In particular, these authors found that quantities such as NH_4^+ production rates were highly sensitive to the distance to the nearest no-flux boundary.

3. How does population density (burrow separation distance) affect concentrations and flushing rates? Is there any evidence of altered irrigation behaviour in response to altered burrow separation? Experiments could measure burrow concentrations and flushing rates with a range of distances to no-flux boundary conditions. Such experiments would help determine whether animal behaviour in narrow tanks is likely to differ from field conditions.

5.6 Port Phillip Bay

Extensive measurements were made in the Port Phillip Bay Environmental Study (PPBES), with the aim of calculating nutrient budgets and inferring nutrient pathways in the system. The final analysis suggested that 70-90% of the loss of nitrogen from the Bay is through the denitrification pathway in the Bay sediments. These rates of denitrification are vital for preventing eutrophication in the Bay.

The single most important discovery of the PPBES is that denitrification in the sediments prevents soluble and available N (ammonia and nitrate) from accumulating in the water column because it is removed from the main Bay environment as nitrogen gas (N_2). (Harris et al. (1996), p.91)

Much has been made of the potential role of burrowing invertebrates in these processes. For example:

A key feature disclosed by PPBES is bioirrigation of the sediments with oxygen rich water through the activities of benthic invertebrates… One of the important results of bioirrigation is to carry dissolved oxygen to sites deep in the sediments (at least to 50 cm) thus facilitating aerobic degradation of organic material carried into the sediments by burrowing and grazing animals. (Harris et al. (1996), p.91)

and

One can think of the burrow system as a great expansion of the sediment-water interface, analagous to a lung. In fact, there is evidence from other sediment studies that the large burrows, such as those of the callianassids in Port Phillip Bay, are just the trunks of an extensive system of finer burrows, so that the lung analogy may be a good one. While some 1-D models have tried to represent the effect of bioirrigation as a non-local transport process, it is not clear that this is an appropriate solution. (Harris et al. (1996), p.174)

Sediment profiles of excess ^{210}Pb and ^{228}Ra deficiency suggested animal activities to a depth of 50 cm (Hancock and Hunter (1999)). Tracer losses from benthic chamber studies in the bay have also indicated that sediment bioirrigation could be occurring to depths of up to 50 cm (Berelson et al. (1999)), and the authors wondered at the cause:

The biological aspects of the various sites should be integrated with the physical data reported here. What are the benthic organisms which produce such high pumping rates…? (Berelson et al. (1996))

A major outcome of the study was the development of a nutrient cycling model which integrated physical and ecological processes (Murray and Parslow (1997)). Sediment denitrification was incorporated into the model using an empirical relationship which suggested high denitrification efficiencies were possible at low sediment respiration rates, with efficiencies dropping at high sediment respiration rates. However the authors stressed the importance of sediment biogeochemistry, and suggested further investigation into the underlying processes:

> *"There is a great deal of scope for further development of process models of sediment biogeochemistry. More use can be made of the existing sediment profile and flux data…"*
> (Murray and Parslow (1997), p.186)

Although some process modelling of nitrification and denitrification was conducted as part of the PPBES, it was limited to a vertical one-dimensional non-local model, and the authors suggested the need to look further at the effects of three-dimensional structure in the sediment. Unfortunately, very little is actually known about this three-dimensional structure in PPB. Certainly, there are thalassinidean shrimp in the bay (*Neocallichirus limosus*, *Biffarius arenosus* and *Callianassa ceramica*) and their burrow structures are well described (Bird et al. (1997)), however there is considerable uncertainty in the density of their population. Early surveys counted *Neocallichirus limosus* as the second most numerous species recorded, yet the more recent surveys have found a substantially reduced population density (Wilson et al. (1998)). It should be noted, however, that surveys were conducted by remote grab samples, which captured only the upper 10cm of sediment. If shrimp were lurking at more distant depths they would not have been recorded, so we can assume that reported population densities were an under-estimate. Consequently, there is insufficient information to determine the nature of the burrow structures across the bay, particularly at depth.

The PPBES field program provided details of porosity, concentration profiles and solute fluxes. Unknown details are the burrow geometry, irrigation behaviour and the spatial distribution of organic matter mineralisation within the sediment. The aim in this work was to use models to determine the range of burrow radii, inter-burrow distances and flushing rates that could explain the measured porewater concentrations and nutrient fluxes. The denitrification efficiency was of particular interest. The one-dimensional process modelling conducted by Murray and Parslow (1997) was unable to explain the very high efficiencies (>80%) recorded in the bay.

The previous case studies considered in this chapter involved contrived circumstances in that in all cases the sediment was mixed vertically prior to shrimp colonisation. For this reason I felt justified in assuming vertically uniform P_{DOC} distributions, an essential assumption if the 1-D radial model is to be valid. I employed this same 1-D approach when modelling PPB sediments, however its validity is questionable given the likely vertical distribution of organic matter within these sediments. In particular, highly labile organic matter will not be uniformly mixed to great depths by the shrimp, as evidenced by the distribution of the short half-life ^{228}Th data from PPB in Chapters 3 and 4. A further difficulty in using the one-dimensional radial approach is that this model provides only the burrow fluxes, yet total sediment fluxes comprise both sediment surface and burrow components. These concerns prompted me to conduct further modelling exercises using a modified version of the model, implemented with full cylinder geometry.

5.6.1 One-dimensional radial model

If a large lung-like structure in the sediment is responsible for the observed denitrification behaviour in PPB, how deep and how dense must these burrows be to achieve this effect? A first attempt to answer this question was made using the one-dimensional radial model. Embedded in the implementation of this model were three main assumptions:

1) Uniform organic matter distribution in the sediment;

2) Nitrification and denitrification zones surrounding burrows are the main sites for these reactions (ie. Nitrification and denitrification occurring just below the sediment surface forms a negligible contribution to the total rates);

3) Steady state conditions with constant partial flushing in permanent burrows.

The conceptual model of this case is a volume of well-mixed sediment irrigated to such a depth that irrigated burrow surface area far exceeds planar sediment-water surface area. The chief drawback with this model is that, although sediment mixing is substantial in the bay, labile organic matter mineralises at such a rate that it is likely to remain concentrated at the very surface of the sediment only. Nevertheless, this approach provides a tangible starting point.

A series of model runs were run spanning a range of DOC production rates, burrow flushing rates, porosity and burrow geometry (see parameter values in Table 5.6).

Table 5.6 Parameter values used in model runs (1440 runs total).

Parameter	Values modelled
ϕ	0.9, 0.65
r_1	0.15, 0.2, 0.3, 0.4, 0.5 cm
r_2	1 ,2, 3, 4, 5, 6 cm
P_{DOC}	20, 50, 100, 200, 500, 700, 900, 1200 nmol/cm^3/d
F_l	48, 24, 24/5 d^{-1}

Given that each run specifies a burrow geometry, porosity and DOC production rate, we can find a burrow length, L (cm), that is required to produce a given areal respiration rate, R_c (nmol C /cm^2/d). The volume of sediment surrounding a burrow is $V = \pi\left(r_2^2 - r_1^2\right)L$, and the surface area implicit in the areal respiration rate is $A = \pi r_2^2$. At steady state the DOC production rate must balance the measured areal respiration rate, so $\phi P_{DOC} V = R_c A$. Substituting in the expressions for V and A and re-arranging we get

$$L = \frac{R_c r_2^2}{\phi P_{DOC}\left(r_2^2 - r_1^2\right)} \qquad \textbf{(5.30)}$$

By prescribing the porosity and the areal respiration rate, the distribution of denitrification efficiencies can be plotted as a function of burrow length, radius and separation distance. In other words, the theoretical relationship between denitrification efficiency and the depth and density of burrows can be explored. It is assumed that all organic matter decomposition takes place within the burrowed layer of the sediment. This assumption is reasonable, as there is no mechanism for significant amounts of organic matter to be transported below the burrowed zone, as burial rates have been shown to be negligible in PPB.

The most detailed denitrification studies were conducted at Site 37 and Site 16 in Port Phillip Bay. These sites were considered typical of two extremes in the Bay: Site 37 had a low areal respiration rate (~20 mmol/m^2/day CO_2) and high denitrification efficiency (>70%), and Site 16 a high respiration rate (>50 mmol/m^2/day CO_2) and lower denitrification efficiency (<50%) (Figure 5.23). These results were found by direct measurement of nitrogen gas accumulation in benthic chambers deployed at the two sites (Heggie et al. (1999)).

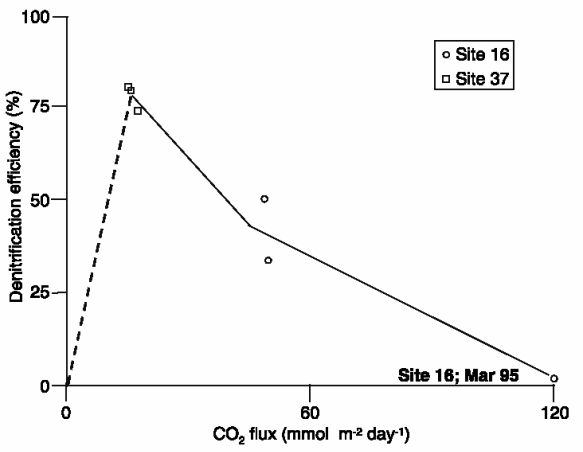

Figure 5.23 Percentage denitrification, measured ($[N_2]/\{[N_2]+DIN\}$) v. CO_2 flux at Site 16 and Site 37, January 1996. (Taken from Heggie et al. (1999)).

The measured field values for porosity and areal respiration rate were used to produce maps of denitrification efficiency as a function of burrow spacing (r_2) and burrow length (calculated from equation (5.30)) from the collection of model runs. This procedure produced 15 maps for each site, as there was a map for each combination of burrow radius (5 values) and flushing rate (3 values). Interpolation between model data points was calculated with Matlab's *interp2* function, using a bicubic interpolation method. Four of the maps for each site are shown in Figure 5.24 and Figure 5.25, and these represent the four extreme cases: (a) minimum r_1 value and maximum F_l value; (b) minimum r_1 value and minimum F_l value; (c) maximum r_1 value and maximum F_l value; (d) maximum r_1 value and minimum F_l value.

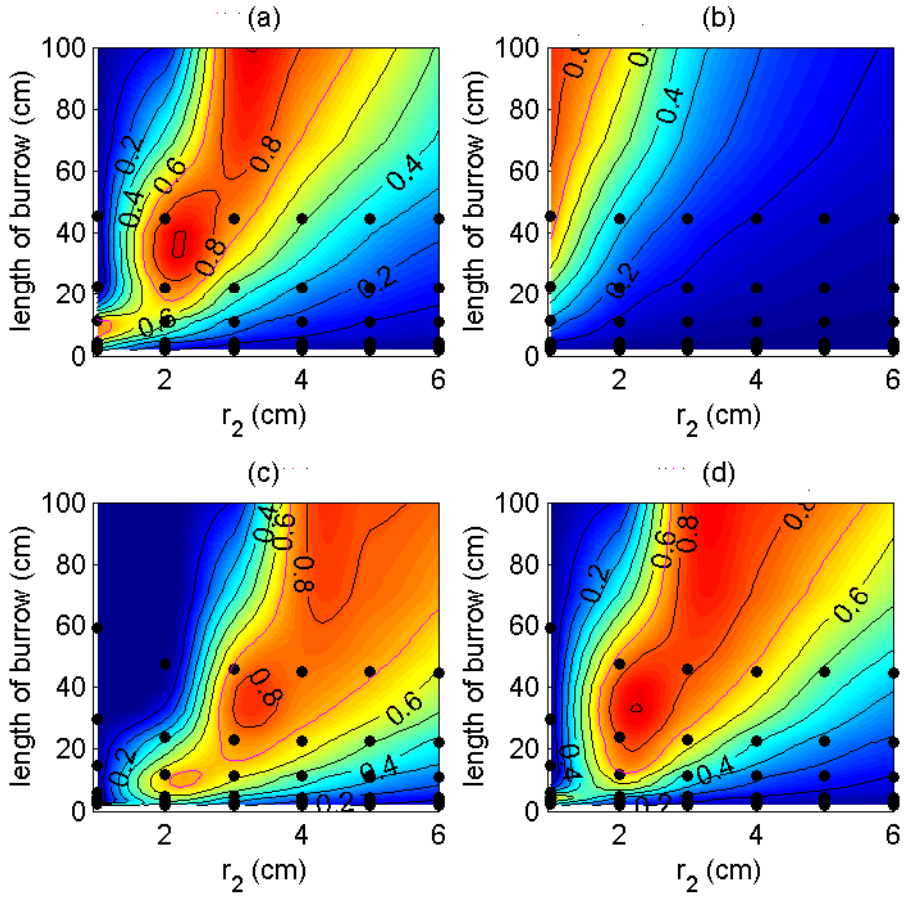

Figure 5.24 Denitrification efficiencies interpolated from model runs (efficiencies represented as fractions rather than percentages). Data points from model runs represented by black circles (some points not shown, as L > 100cm). Sediment porosity and areal respiration rate have been set at values typical for Site 37 in Port Phillip Bay ($\phi = 0.9$, $R_c = 20$ mmol/m2/day), burrow length has been calculated from equation (5.30). The purple line marks the 70% denitrification efficiency contour (efficiencies typically exceed this value at Site 37). (a) $r_1 = 0.15$cm, $F_1 = 48$ day^{-1}; (b) $r_1 = 0.15$cm, $F_1 = 24/5$ day^{-1}; (c) $r_1 = 0.5$cm, $F_1 = 48$ day^{-1}; (d) $r_1 = 0.5$cm, $F_1 = 24/5$ day^{-1}.

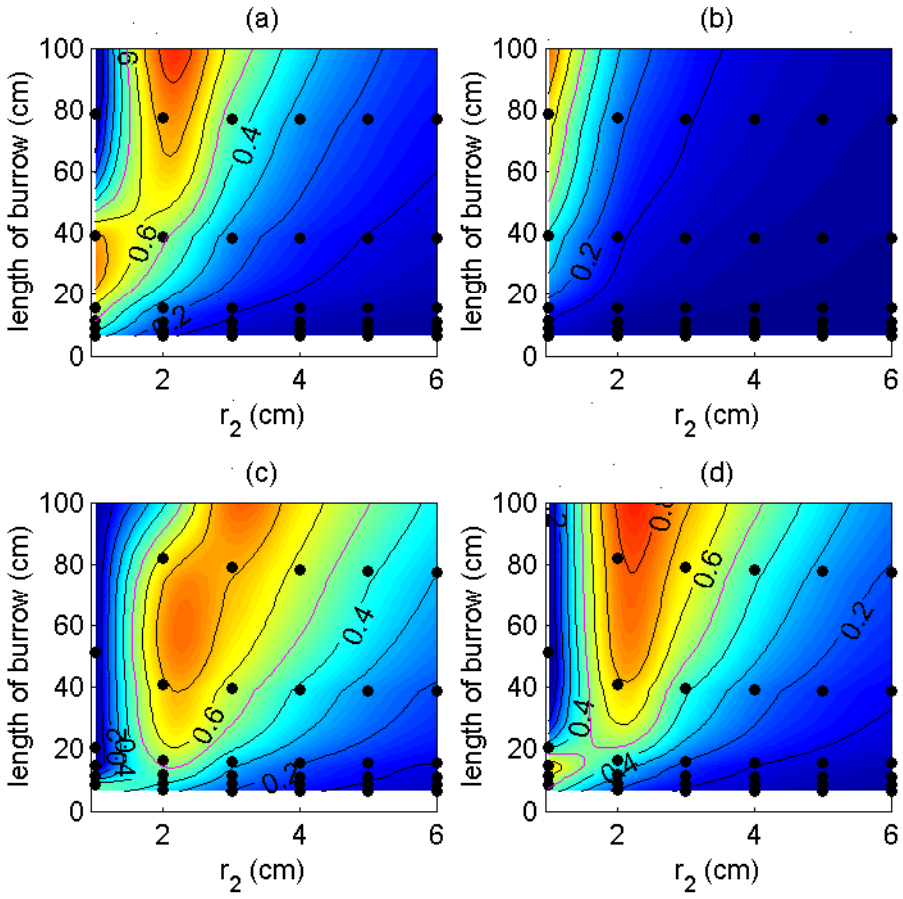

Figure 5.25 Denitrification efficiencies interpolated from model runs (efficiencies represented as fractions rather than percentages). Data points from model runs represented by black circles (some points not shown, as L > 100cm). Sediment porosity and areal respiration rate have been set at values typical for Site 16 in Port Phillip Bay ($\phi = 0.65$, $R_c = 50$ mmol/m2/day), burrow length has been calculated from equation (5.30). Purple lines mark the 50% denitrification efficiency contour, which is a typical value measured at this site. (a) $r_1 = 0.15$cm, $F_1 = 48$ day^{-1}; (b) $r_1 = 0.15$cm, $F_1 = 24/5$ day^{-1}; (c) $r_1 = 0.5$cm, $F_1 = 48$ day^{-1}; (d) $r_1 = 0.5$cm, $F_1 = 24/5$ day^{-1}.

There are three factors to consider in interpreting these diagrams: burrow geometry, flushing rate and areal respiration rate. Generally speaking, the more densely populated an area (ie the lower the r_2 value), the higher the denitrification efficiency. This generalisation breaks down as soon as a critical r_2 (referred to as r_{peak} in the following discussion) is reached, and denitrification efficiency drops off rapidly below this point. The explanation is that at very low r_2 values there are insufficient anoxic regions separating burrows to yield significant denitrification rates, so increasing r_2 increases denitrification until $r_2 = r_{peak}$, beyond which the volume of anoxic sediment producing NH_4^+ begins to overwhelm the volume of oxic sediment able to nitrify this NH_4^+. The value of r_{peak} is dependent on burrow radius, flushing rate and burrow length (or respiration rate per unit volume of sediment). Lowering r_1 has the effect of

lowering r_{peak}, but the extent to which r_1 changes r_{peak} is highly dependent on flushing rate. For example, the difference between Figure 5.24(a) and Figure 5.24(c) is much smaller than the difference between Figure 5.24(b) and Figure 5.24(c). Here there are two effects: decreasing the flushing rate lowers the value of r_{peak} , but it can slightly increase the peak denitrification rate (compare Figure 5.24(c) and Figure 5.24(d)). Reducing the flushing rate reduces the supply of oxygen to the sediment, and so reduces volume of nitrifying sediment and hence r_{peak}. However, the reduced flushing rate also effectively 'traps' NO_3^- into the sediment as it is not being flushed out of the burrow as rapidly, and so provides more opportunity for the NO_3^- to be converted to nitrogen gas.

In terms of specific predictions for PPB, the model suggests that at Site 37, denitrifying efficiencies exceeding 70% could occur from a range of burrow density, burrow length and flushing rate combinations. For example, burrows as shallow as 10cm can allow sufficiently high denitrification rates, if they are separated by approximately 4cm (r_2 = 2cm). If burrows are as deep as 50cm (as widely speculated in the final report), burrow separation distances of 4cm to 11cm can yield sufficiently high denitrification rates.

Are these numbers physically realistic? Firstly, it should be noted that these specific burrow lengths and separation distances are based on a burrow radius of 0.5cm, which is typical of thalassinidean burrows. The population density of shrimp measured in the Bay in 1995 were 21 m^{-2} for *Biffarius arenosus* (sandy sediments) and 10 m^{-2} for *Neocallichirus limosus* (muddy sediments) (Bird et al. (1997)). The relationship between burrow density (N m^{-2}) and burrow separation distance ($2r_2$) is given by $N\pi r_2^2 = 1$, so r_2 = 2cm and r_2 = 5.5cm correspond to burrow densities of approximately 800 burrows/m^2 and 100 burrows/m^2. Even allowing for the fact that there are multiple burrow shafts per individual (and that Bay populations are likely to be underestimated by grab sampling techniques), clearly the measured population density falls well short of the density required by the model to produce the very high denitrification rates. It is certainly unrealistic to contemplate sediment filled with 1cm diameter burrows at a density of 800 per m^2. It is more possible to consider sediment containing 100 burrows/m^2, as these densities are not uncommon for thalassinidean shrimp. It is not clear, however, that such a burrow density would be maintained to a depth of 50cm (it is more typical that animals maintain multiple openings to the sediment surface, and a sparser burrow network at depth).

Turning to the model runs based on Site 16 (Figure 5.25), we see that there is a far narrower range of burrow geometry and flushing combinations that can yield high denitrification efficiencies. Thus, qualitatively, it matches the field observations that a higher areal respiration rate is correlated with lower denitrification efficiencies. When the respiration rate is reduced even further to 120 mmol/m²/day (measured in March 1995 at Site 16, see Figure 5.23), there are even fewer regions of high denitrification efficiency (Figure 5.26).

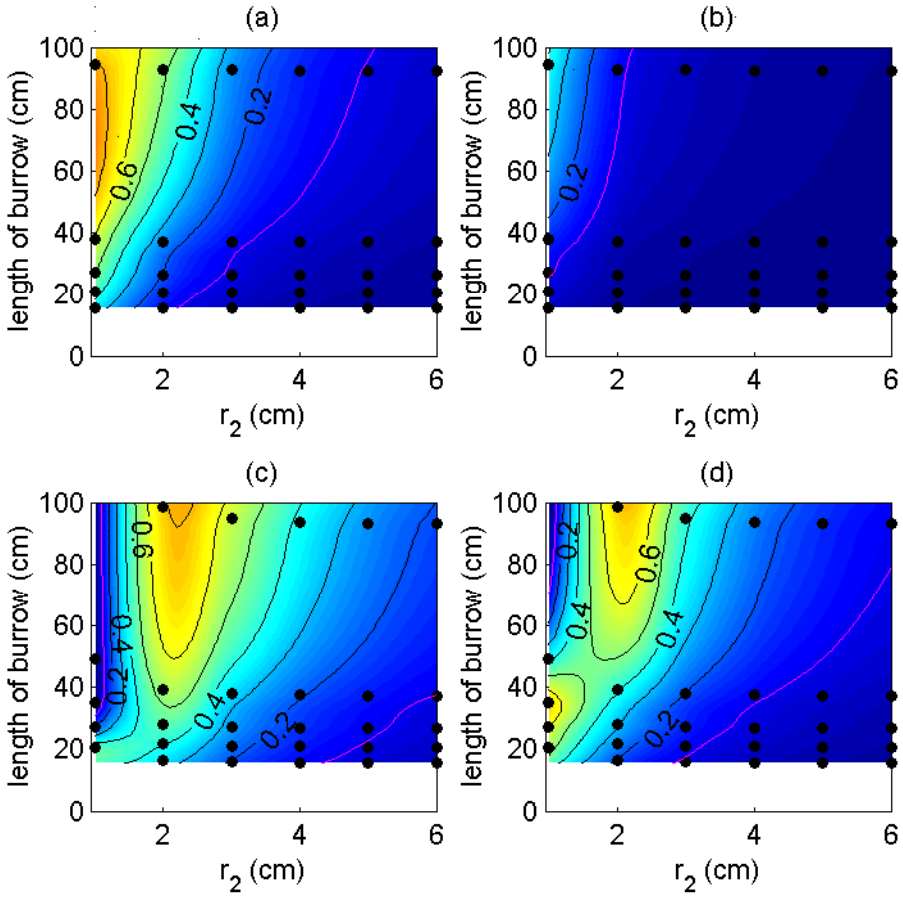

Figure 5.26 Denitrification efficiencies interpolated from model runs (efficiencies represented as fractions rather than percentages). Data points from model runs represented by black circles (some points not shown, as L > 100cm). Sediment porosity and areal respiration rate have been set at values typical for Site 16 in Port Phillip Bay ($\phi = 0.65$, R_c = 120 mmol/m2/day), burrow length has been calculated from equation (5.30). Purple lines mark the 10% denitrification efficiency contour – the measured field denitrification efficiency was under 10%. (a) r_1 = 0.15cm, F_1 = 48 day^{-1}; (b) r_1 = 0.15cm, F_1 = 24/5 day^{-1}; (c) r_1 = 0.5cm, F_1 = 48 day^{-1}; (d) r_1 = 0.5cm, F_1 = 24/5 day^{-1}.

The seasonal changes in denitrification efficiency at Site 16 provided some of the most compelling evidence for the empirical function reported in the PPBES relating denitrification efficiency to sediment respiration rate. Site 16 experienced dramatic changes in sediment respiration rate and denitrification efficiency, and the two were

seen to be inversely related. Just over a doubling in sediment respiration rate (from 50 mmol/m^2/day to 120 mmol/m^2/day) corresponded to a reduction in denitrification efficiency from around 50% to below 5% (Figure 5.23). Note that while the model produces the same qualitative picture (reduced denitrification efficiency with increased respiration rate, as seen by comparing Figure 5.25 and Figure 5.26), the effect is less pronounced than the field measurements. For example, geometry configurations that yielded ~50% efficiency in Figure 5.25 typically produce efficiencies of 25%-30% in Figure 5.26 – a reduction by a factor of two, as compared to a factor of ten measured in the field. However this analysis is not particularly helpful, as such a dramatic change in sediment respiration rate is likely to have an impact on the animals living in the sediment. Indeed, it is likely that population density would fall (r_2 increase) in response to increasing levels of anoxia in the sediment. Under these circumstances, further drops in denitrification efficiency can be explained by the model results.

Due to the extensive nature of the PPB investigations, there are other checks we can make against the model predictions. In particular, the field studies measured pore water concentrations in sediment cores and benthic chamber fluxes at each site (Nicholson et al. (1996)). Figure 5.27 shows predicted NH_4^+ and NO_3^- concentrations and fluxes for r_1 = 0.3cm and F_l = 24 day^{-1} (middle of the range of r_1 and F_l values modelled) with porosity and respiration rate set to typical Site 37 values (ϕ = 0.9, R = 20 mmol m^{-2} day^{-1}). The 70% denitrification efficiency contour has been superimposed on these maps, to show the region of r_2 and L values which match the field denitrification rates. These maps were used to produce the data shown in Table 5.7, where field and modelled concentrations and fluxes are compared.

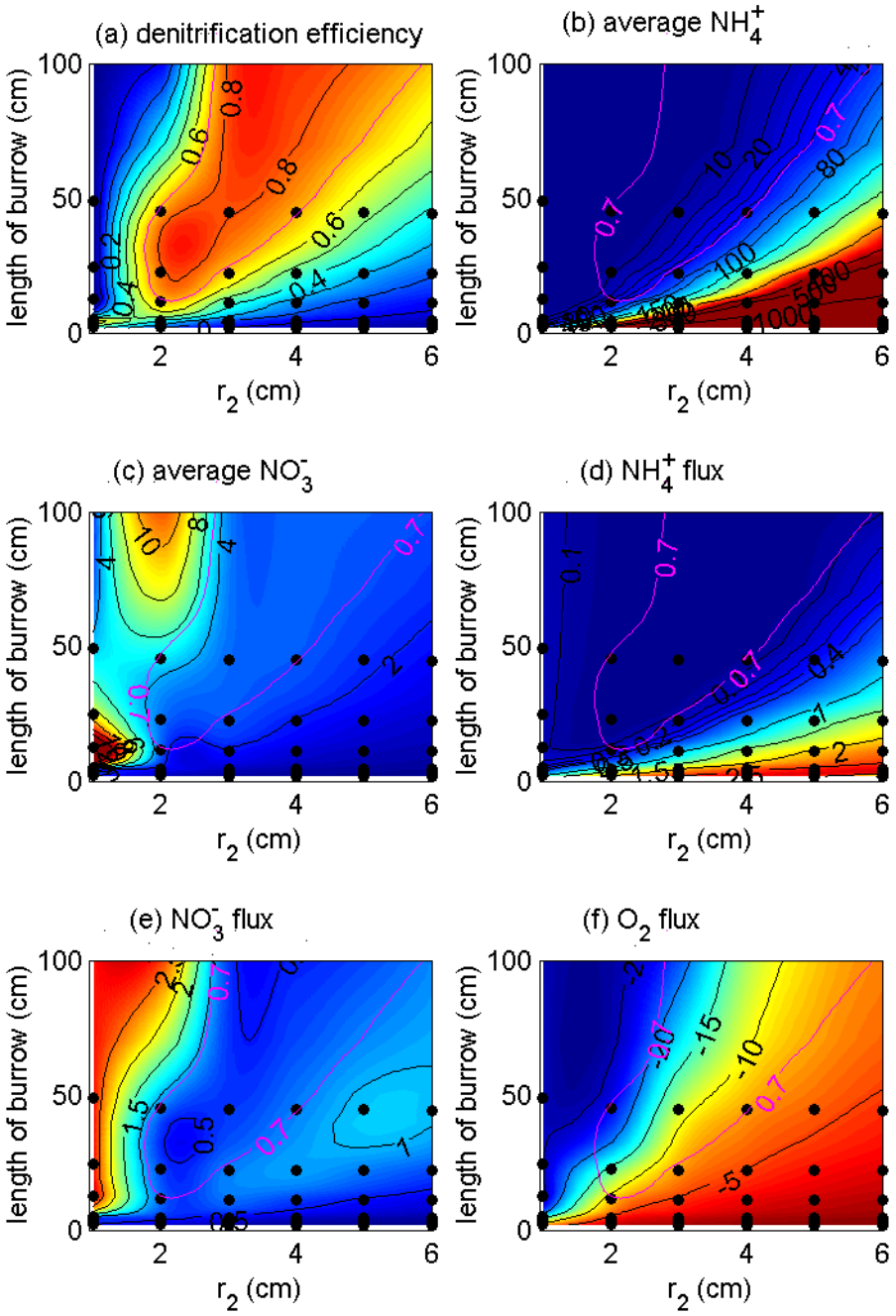

Figure 5.27 Plots of denitrification efficiency, average NH_4^+, average NO_3^-, NH_4^+ flux, NO_3^- flux and O_2 flux against r_2 and burrow length (calculated from equation (5.30)). Respiration rate and porosity were fixed at typical values for Site 37 ($\phi = 0.9$, $R = 20$ mmol/m^2/day), $r_1 = 0.3$ cm and $F_l = 24$ day^{-1}. The purple line shows the 70% denitrification efficiency contour (efficiencies typically exceed this value at Site 37). Units are µmol/L for concentration and mmol m^{-2} day $^{-1}$ for fluxes. Denitrification efficiencies are represented as a fraction rather than a percentage.

Table 5.7 Comparison between measured and modelled concentrations and fluxes for Site 37 in PPB. Numbers are approximate only, having been read by eye from Figure 5.27 (above) and bar graphs from Figure 31 in Nicholson et al. (1996).

	Modelled range within 70% denitrification efficiency contour	**Measured range**
Average NH_4^+	<10 to 50 µmol/L	10 to 30 µmol/L
Average NO_x	2 to 6 µmol/L	2 to 5 µmol/L
NH_4^+ flux	0.1 mmol m^{-2} day^{-1}	0 to 0.3 mmol m^{-2} day^{-1}
NO_x flux	0.5 to 1 mmol m^{-2} day^{-1}	-0.2 to 0.3 mmol m^{-2} day^{-1}
O_2 flux	-20 to -8 mmol m^{-2} day^{-1}	-28 to -15 mmol m^{-2} day^{-1}

In general, the comparison between field and model concentrations and fluxes are good (Table 5.7), although the model over-predicts the NO_x flux (at least 0.5 mmol m^{-2} day^{-1} modelled compared to at most 0.3 mmol m^{-2} day^{-1} measured).

Tracer studies were also used to estimate *in situ* sediment irrigation rates in PPB (Berelson et al. (1999); Hancock et al. (1997)). Irrigation rates can be calculated for each model run, providing another point of comparison with field data. For each model run, we have the burrow geometry (radius r_1 and length L calculated from equation (5.30) for a specified respiration rate) and a burrow flushing rate constant, F_l. The volumetric flushing rate per unit area (L/m²/day) is:

$$Q = \pi r_1^2 L F_l N \qquad \textbf{(5.31)}$$

where N is the number of burrows per unit area.

Again, choosing r_1 = 0.3 cm and F_l = 24 day^{-1}, the volumetric flushing rate per unit area have been plotted against r_2 and L (Figure 5.28). Superimposed on this graph are the 70% and 50% denitrification contours for Site 37 and Site 50 respiration rates respectively. Based on this graph, flushing rates of between 60 and 300 L/m²/day are predicted for Site 37, and over 100 L/m²/day for Site 16. These rates can be directly compared to irrigation rates inferred in Berelson et al. (1999) and Hancock et al. (1997).

Berelson et al. (1999) measured the loss of deuterium from benthic chambers, and used a diffusion and non-local exchange model to infer the rate at which chamber water is pumped into the sediment. Their rates were in units of mL/h, which I have converted to L/m²/day, using the chamber area of 730cm². They deduced that flushing rates were 52 to 64 L/m²/day to a depth of 20-25cm at Site 37, which sits across the lower boundary of the 60 to 180 L/m²/day range inferred from Figure 5.28 (found by

intersecting the region of >70% denitrification efficiency with the burrow length region of 20-25 cm). Berelson et al. (1999) deduced a much higher flushing rate to a much greater depth at Site 16, although the result was inconclusive as there was the possibility of chamber leakage at this site (based on a comparison between Cs and deuterium losses from the chamber). Hancock et al. (1997) analysed radium balances to derive a flushing rate of 59 L/m²/day, which is the same as the rate calculated by Berelson et al. (1999).

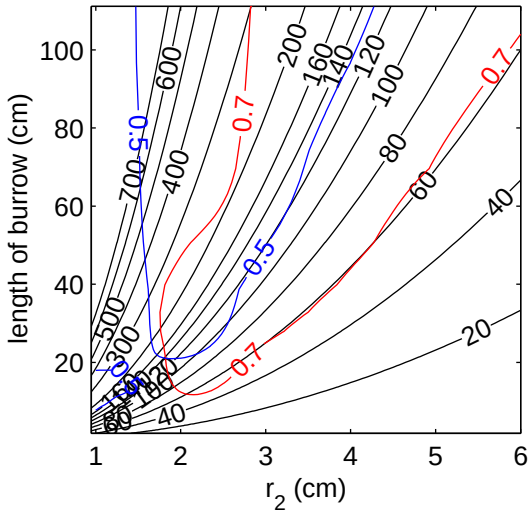

Figure 5.28 The black contours show flushing rates (L/m²/day) for burrows with r_1 = 0.3cm and F_l = 24 day^{-1}. The red contour is the 70% denitrification contour for a typical Site 37 respiration rate and porosity, and the blue contour is the 50% denitrification contour for a typical Site 16 respiration rate and porosity (calculated from model runs using r_1 = 0.3cm and F_l = 24 day^{-1}; eg. the red contour comes from Figure 5.27 (a))

Berelson et al. (1999) stated that their estimated flushing rates were in agreement with measurements of *Callianassa truncata* flushing rates made by Forster and Graf (1995), yet I find it hard to draw the same conclusion. Forster and Graf (1995) measured areal flushing rates of 5.3 L/m²/day (2.8 L/m²/day regular irrigation + 2.5 L/m²/day irregular irrigation) for *Callianassa truncate*, which are well below the flushing rates discussed in the previous paragraph. Berelson et al. (1999) chose to convert all literature flushing rates to a flushing rate across their benthic chamber area (730 cm²), so a rate of 5.3 L/m²/day converts to 16.2 mL/h (across 730cm²). Yet Berelson et al. (1999) cited a converted rate of 480 mL/h for *Callianassa truncata*, which is roughly a factor of 30 too high. I can only assume Berelson et al. (1999) made a mistake in their calculation. While Berelson et al. (1999) concluded that their irrigation rates compared well with measurements of thalassindean pumping rates, I can only conclude that the

rates are extremely high, and are certainly not physically realistic given our understanding of typical thalassinidean population densities and flushing rates.

Forster and Graf (1995) measured a population density of 21 ind/m^2, and estimated that 1.6 m^2 of burrow surface lie beneath each m^2 of surface sediment. Calculations of burrow surface area for the range of model runs are shown in Figure 5.29. The estimate from Forster and Graf (1995) falls at the low end of model burrow surface area.

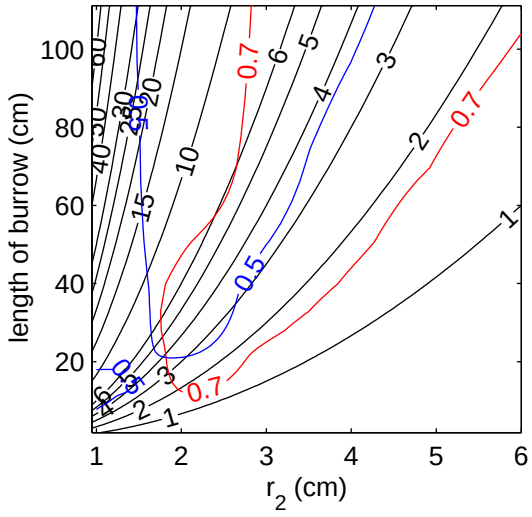

Figure 5.29 The black contours show burrow surface area (m^2/m^2) for burrows with r_1 = 0.3cm. The red contour is the 70% denitrification contour for a typical Site 37 respiration rate and porosity, and the blue contour is the 50% denitrification contour for a typical Site 16 respiration rate and porosity (calculated from model runs using r_1 = 0.3cm and F_l = 24 day^{-1}; eg. the red contour comes from Figure 5.27 (a))

The conclusions from these results are unclear. It seems that the one-dimensional radial burrow model can explain the measured denitrification rates, porewater concentrations, porewater fluxes and to some extent flushing rates. However, the implied burrow density and flushing rates do not appear physically realistic. Certainly, they are not realistic for thalassinidean shrimp populations: measured flushing rates and population densities are far lower than those predicted by the model results. While PPB shrimp densities are not high enough, the total benthic fauna density exceeds 1000 ind/m^2 (Wilson et al. (1998)), and so it is conceivable that other animals may be important. The problem with this conclusion is that only the thalassinidean shrimp build permanent, irrigated burrows to the required depths of greater than 20 cm. Another possibility is that smaller animals build burrows extending out from the main burrows of thalassinidean shrimp. Thus a higher density of burrows could be maintained to considerable depths. Very little is known about the burrow structures in

Port Phillip Bay sediments; useful future work would be to investigate the sediment burrow networks more thoroughly, perhaps by resin-casting.

5.6.2 5 species cylinder model

There are many drawbacks of the one-dimensional burrow model used so far. Two issues of particular importance are:

1. It calculates only the burrow contribution to total fluxes, where in reality the total flux between the sediment and overlying water is the sum of the flux across burrow surfaces and the planar sediment-water interface.

2. The burrow flux estimates will be inaccurate, particularly if shallow burrows are being modelled, as they fail to account for interactions with surface reactions which will alter concentrations at depth.

For these reasons, it is desirable to take a look at a full cylinder model in order to more completely estimate the relative roles of surface and burrow processes. I've implemented such a model to make a comparison with the 1-D radial model results.

The nitrogen model outlined in equations (5.3) to (5.10) was modified in three ways: an extra dimension (vertical distance z) was included in the diffusion equation, a zero-flux boundary condition was prescribed at the maximum z value, and SO_4^{2-} and HS^- concentrations were excluded (reducing the number of chemical species from 7 to 5). Model parameters and solution method remained the same. A 5-species version of the one dimensional model was also constructed, and comparisons with the full 7-species version were very good (eg. Figure 5.30).

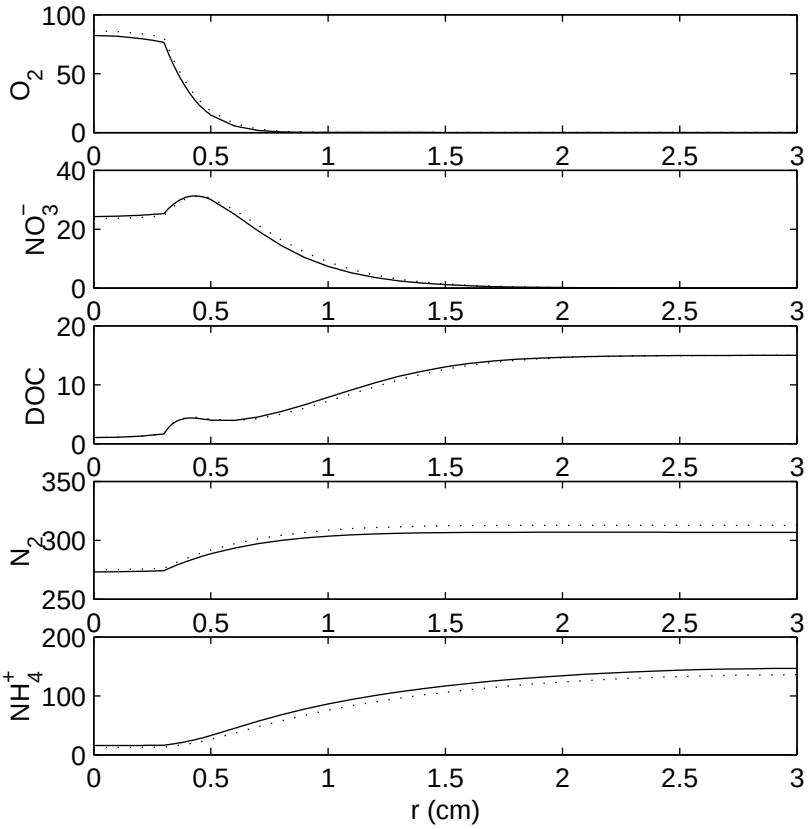

Figure 5.30 Comparison between 5-species and 7-species 1-D radial models. Solid line: 7-species model; Dotted line: 5-species model.

5.6.2.1 Comparisons between 1-D and 2-D models

As a first step, the results were compared between 1-D and 2-D models, where in both cases a uniform P_{DOC} = 150 μmol/L/day had been prescribed. The length of the burrow was set to 10cm for the 2-D model runs. Four parameter combinations were tested:

1. r_2 = 3 cm, F_l = 24 day^{-1};
2. r_2 = 3 cm, F_l = 24/5 day^{-1};
3. r_2 = 5 cm, F_l = 24 day^{-1};
4. r_2 = 5 cm, F_l = 24/5 day^{-1}.

Using a porosity typical of site 37 at PPB (ϕ = 0.9), and assuming P_{DOC} = 0 below z = 10cm, the areal respiration rate is 13.5 mmol/m^2/day.

At the base of the 2-D model (i.e. at a depth of 10cm), the radial concentration distribution was found to be essentially the same as that produced by the 1-D model (Figure 5.31), which suggests that below this depth there is negligible surface influence, and so the 1-D and 2-D models would produce the same results in the L>10cm region.

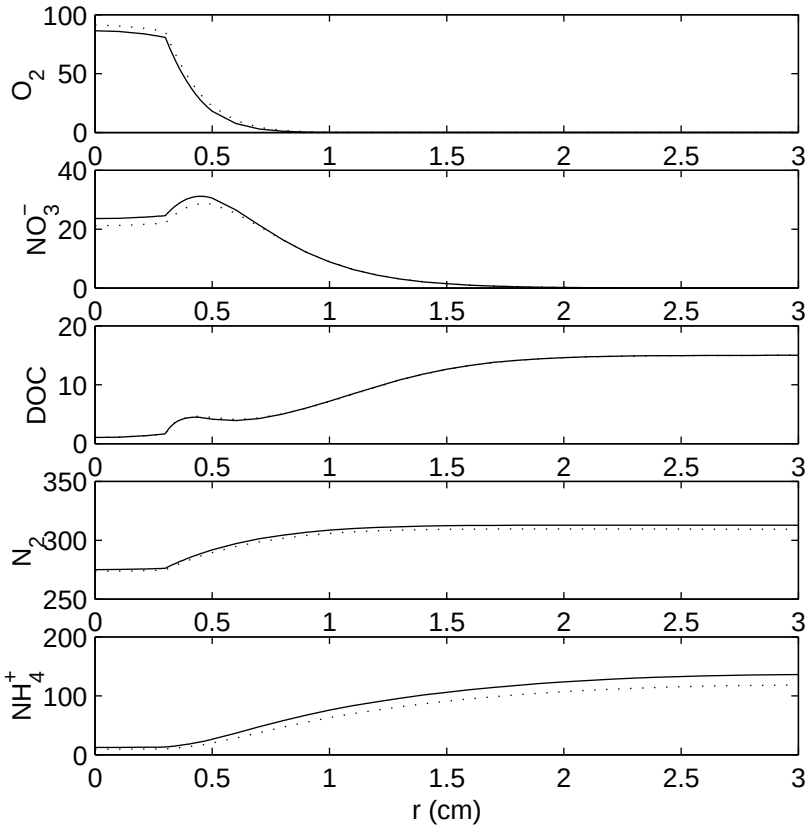

Figure 5.31 Comparison between 1-D and 2-D 5-species radial models. Solid line: 1-D model; Dotted line: 2-D model at depth of 10cm. Units are %saturation for O_2 and μmol/L for all other species.

Within this top 10cm, however, the planar sediment surface can make significant contribution to the sediment-water exchange rates. The cylinder model flux formulae are (modified from Aller (1980) to represent flux per unit of planar sediment surface):

$$J = J_z + J_{r\_2D} \qquad \textbf{(5.32)}$$

where

$$J_z = -\frac{\phi D_s 2\pi \int_{r_1}^{r_2} \frac{\partial C}{\partial z} r \, \mathrm{d}r}{2\pi \int_0^{r_2} r \, \mathrm{d}r}$$

$$J_{r\_2D} = -\frac{A_r}{A_z} \frac{\phi D_s \int_0^L \frac{\partial C}{\partial r} \mathrm{d}z}{\int_0^L \mathrm{d}z}$$

where A_z is the surface area of the cylinder top at $z = 0$ and A_r is the surface area of the burrow wall.

Alternatively, because the system is at steady state, the total flux for a species can be found by integrating that species' reaction term:

$$J = -\frac{2\int_0^L \int_{r1}^{r2} \phi R r \, \mathrm{d}r \, \mathrm{d}z}{r_2^2} \qquad \textbf{(5.33)}$$

The spatial resolution of the 2-D model was coarse (1mm), with the exception of a 3mm band at the burrow wall, which had a grid size of 0.1 mm in the *r*-direction (and 1mm in the vertical). For this reason, fluxes calculated from the gradient at the burrow wall will be more reliable than fluxes calculated from the gradient at the sediment surface. Hence the expression for J_{r_2D} in equation (5.32) was used to calculate the burrow component of the flux, and equation (5.33) was used to calculate the total flux, J. The difference between the two is the surface component of the flux, J_x.

The planar sediment surface has an influence on flux calculations in two ways: directly, as material diffuses across this surface (J_z); and indirectly, as the surface reactions affect the concentrations at depth, and so influence the value of J_{r_2D}. The significance of both these effects can be assessed by comparing flux estimates from equations (5.32) and (5.33) with fluxes calculated from equation (5.15).

The ratio, J_z/J for the four cases shows that the surface component of the total flux is substantial, particularly for a low population density of poorly flushed burrows (Table

5.8). This presents a serious problem for the 1-D model, and this limitation needs to be borne in mind when interpreting its results.

Table 5.8 J_z/J calculations from 2-D model runs, demonstrating the relative importance of the surface contribution to the total flux.

	O_2	NO_3^-	DOC	N_2	NH_4^+
r_2 = 3 cm, F_l = 24 day^{-1}	0.46	0.36	0.74	0.31	0
r_2 = 3 cm, F_l = 24/5 day^{-1}	0.71	0.73	0.85	0.59	0.12
r_2 = 5 cm, F_l = 24 day^{-1}	0.71	0.61	0.89	0.65	0.38
r_2 = 5 cm, F_l = 24/5 day^{-1}	0.88	0.90	0.94	0.84	0.50

Knowing that the model can only hope to represent the burrow component of the fluxes between the sediment and overlying water, how well does the 1-D model predict these fluxes? Results in Table 5.9 show that the surface has a significant effect on the burrow flux values. Most notable is the difference in NH_4^+ fluxes predicted by the two models. The presence of the sediment surface provides more sites for nitrification reactions, hence lowering NH_4^+ concentrations within the sediment and depth. Consequently, the NH_4^+ gradient between the burrow wall and surrounding sediments is less, and so the burrow flux is less. These interactions are not picked up by the 1-D model, so it seriously over-estimates the burrow component of the NH_4^+ flux.

Table 5.9 J_r/J_{r_2D} calculations. J_r was calculated from the 1-D model data using equation (5.14), and J_{r_2D} was calculated from the 2-D model data using the expression in (5.32).

	O_2	NO_3^-	DOC	N_2	NH_4^+
r_2 = 3 cm, F_l = 24 day^{-1}	1.16	1.48	1.00	1.35	2.12
r_2 = 3 cm, F_l = 24/5 day^{-1}	0.94	1.03	0.99	1.14	3.15
r_2 = 5 cm, F_l = 24 day^{-1}	1.22	1.52	0.94	1.33	5.53
r_2 = 5 cm, F_l = 24/5 day^{-1}	0.93	0.99	1.00	1.18	6.82

The combined effects of the direct and indirect surface influences indicate problems for the 1-D model. J_r/J calculations (Table 5.10) show that the 1-D model can produce some flux estimates that are 10% of the total flux (eg. NO_3^-), and other flux estimates which are more than treble the total flux (eg. NH_4^+). These effects are most pronounced for lower flushing rates and burrow densities.

Table 5.10 J_r/J calculations. J_r was calculated from the 1-D model data using equation (5.14), and J was calculated from the 2-D model data using the expression in (5.32).

	O_2	NO_3^-	DOC	N_2	NH_4^+
r_2 = 3 cm, F_l = 24 day^{-1}	0.62	0.95	0.26	0.93	2.20
r_2 = 3 cm, F_l = 24/5 day^{-1}	0.27	0.28	0.15	0.47	2.76
r_2 = 5 cm, F_l = 24 day^{-1}	0.36	0.59	0.10	0.46	3.40
r_2 = 5 cm, F_l = 24/5 day^{-1}	0.11	0.10	0.06	0.19	3.39

So is it all bad news? It must be remembered that away from the surface (certainly 10cm away), the 1-D and 2-D models are identical. This means that the 1-D model will accurately predict the 2-D concentrations at depth, and it will also generate the correct burrow fluxes at these depths. Difficulties only arise when the bulk of the burrow lies within the sediment layer which is influenced by the sediment surface.

Given the level of speculation within the PPB reports that very deep (~50 cm) burrows were responsible for high denitrification rates, it seemed reasonable to neglect the sediment surface and analyse the extent to which burrows could be contributing to these processes. The 1-D burrow model was an ideal tool for this purpose, as many runs could be executed to cover a broad range of parameter combinations. Such an extensive exploration would not have been possible with the slower cylinder model.

The extent to which the surface is important, in terms of predicted nitrification and denitrification efficiencies, strongly depends on the burrow geometry and flushing rate. The 1-D model performs best under high burrow density and flushing rate conditions, worsening substantially as both of these parameters decrease in value (Table 5.11). While the extent of the difference varies, the direction is always the same: the 1-D radial model always underestimates nitrification and denitrification efficiencies. Given that I was using the 1-D model to see if particularly high values were possible, the model results represented a cautious analysis: any predicted denitrification rate represents a *minimum* estimate for that particular model geometry and flushing rate.

Table 5.11 Nitrification and denitrification efficiencies produced from 1-D and 2-D models. In all cases the P_{DOC} is uniform, with a value of 150 μmol/L/day.

	1-D nitrification efficiency	2-D nitrification efficiency	1-D denitrification efficiency	2-D denitrification efficiency
r_2 = 3 cm f_l = 24 day^{-1}	88%	94%	60%	65%
r_2 = 3 cm f_l = 24/5 day^{-1}	30%	74%	24%	51%
r_2 = 5 cm f_l = 24 day^{-1}	42%	82%	23%	50%
r_2 = 5 cm f_l = 24/5 day^{-1}	11%	73%	8.5%	44%

5.6.3 Summary

The emphasis in the PPBES reports was on the physical changes brought about by benthic fauna: redistribution of organic matter and the irrigation of sediments (use of the 'lung' analogy). Chemical changes such as burrow lining, animal excretion and microbial stimulation were also mentioned. This prompts the question of the relative roles of physics and chemistry. Here a modelling approach has been used to assess whether physical changes alone, in the form of altered geometry of the sediment-water interface due to burrows, could explain the observations. A one-dimensional analysis demonstrated that a high areal density of deep well-flushed burrows could explain the observed porewater concentrations and fluxes in PPB, however the required burrow density and flushing rates were too high to be physically realistic.

A two-dimensional analysis illustrated the drawbacks of the one-dimensional approach, showing that the inclusion of the sediment surface makes a substantial difference to model predictions. Nitrification and denitrification rates were always under-estimated in the 1-D model, although by differing amounts. Thus the usefulness of the 1-D model is limited to the fact that thousands of runs can be run with relative ease, which is not possible for the present version of the 2-D model. A practical compromise is to use the 1-D model to conduct a thorough search of the parameter space, and then employ the 2-D model to concentrate on specific cases of interest. Away from the surface influence, the 1-D and 2-D models are identical, and so the 1-D model is a good tool for calculating concentrations and burrow fluxes at depth.

A question that deserves further attention is the role of heterogeneous organic matter distribution in the sediment. In these model runs a uniform P_{DOC} distribution has been

assumed, which is highly unlikely in real sediments. It is more realistic to expect high organic matter content in a thin surface layer, and perhaps lining the burrow wall (which I partially addressed in previously sections). A related question is: what is the source of NH_4^+ at depth? Is it produced at depth from organic matter or does it diffuse down from a thin layer of labile organic matter at the surface? These questions could be tackled relatively easily using this model.

5.7 Conclusions

In this chapter I integrated information from a range of sources to model experimental and field observations from three thalassinidean shrimp studies. The work, while identifying divergences between observations and model results, also pointed to some important methodological considerations when conducting experiments on these creatures. In particular, it underlines the need for transport assumptions and conclusions to be made more explicit in experimental studies. In addition, a greater emphasis on budgets and flows between pools of nutrients would be beneficial. At a larger scale, the emphasis in the PPBES on quantifying not just the pools, but also the exchanges between pools in the system proved to be invaluable in interpreting Bay-wide processes.

Burrow ventilation has been invoked as an explanation for high denitrification efficiencies in PPB. The modelling in this chapter represents an attempt to yield the expected changes from simple assumptions about burrow irrigation. While burrows certainly make a large difference to nitrification and dentrification rates, it was found in PPB at least they are unlikely to be the sole contributor. This would suggest that other hypothesised factors, such as the high concentrations of microphytobenthos are likely to be significant contributors to these rates. Another possibility not explored is that of anoxic nitrate production during manganese reduction, which would feed higher denitrification rates (Hulth et al. (1999)).

The work in this chapter is by no means comprehensive, and it has opened up many avenues for future research. In particular, more work should be done on the role of heterogeneous organic matter distribution. I conducted some model runs in Sections 5.5.1 and 5.5.2, where heterogeneous mineralisation rates were applied to the burrow irrigation model. These limited examples suggested that organic matter heterogeneity coupled with heterogeneous oxygen injection to the sediment can yield very different outcomes, especially in terms of total nitrification and denitrification rates. More

investigations along these lines are required. In particular, heterogeneous organic matter distributions should be incorporated into the full cylinder model. Recent work by Furukawa et al. (2001) has done this and found that the cylinder (or more complicated microenvironment) model is an excellent tool for exploring standard assumptions about organic matter and C/N ratio distributions in sediments.

Throughout this chapter I've limited my approach to steady state model solutions, yet dynamic considerations are likely to be important. In particular, the start-up effects associated with new burrow formation should be investigated.